International Journal of Nanomedicine

Dovepress
open access to scientific and medical research

Open Access Full Text Article

ORIGINAL RESEARCH

Renal interstitial fibrosis induced by high-dose mesoporous silica nanoparticles via the NF-κB signaling pathway

This article was published in the following Dove Press journal:
International Journal of Nanomedicine
18 December 2014
Number of times this article has been viewed

Xi Chen[1,2]
Wang Zhouhua[1]
Zhou Jie[1]
Fu Xinlu[3]
Liang Jinqiang[3]
Qiu Yuwen[3]
Huang Zhiying[1,3]

[1]School of Pharmaceutical Sciences, Sun Yat-sen University, Guangzhou, People's Republic of China; [2]Pharmaceutical Department, The First Affiliated Hospital of Zhengzhou University, Zhengzhou, People's Republic of China; [3]Center of Laboratory Animals, Sun Yat-sen University, Guangzhou, People's Republic of China

Abstract: Previous studies have indicated that the nephrotoxicity induced by mesoporous silica nanoparticles (MSNs) is closely related to inflammation. Nuclear factor kappa B (NF-κB), a common rapid transcription factor associated with inflammation, plays an important role in the process of many kidney diseases. Acute toxicity assessment with a high-dose exposure is critical for the development of nanoparticle, as a part of standardized procedures for the evaluation of their toxicity. The present study was undertaken to observe the acute toxicity, predict the potential target organs of MSNs injury, and test the hypothesis that the NF-κB pathway plays a role in mediating the acute kidney injury and renal interstitial fibrosis in mice induced by MSNs. Balb/c mice were intraperitoneally injected with MSNs at concentrations of 150, 300, or 600 mg/kg. All of the animals were euthanized 2 and 12 days after exposure, and the blood and kidney tissues were collected for further studies. In vitro, the cytotoxicity, fibrosis markers, and NF-κB pathway were measured in a normal rat kidney cell line (NRK-52E). Acute kidney injury was induced by MSNs in mice after 2 days, some renal tubules regenerated and renal interstitial fibrosis was also observed. The expression of fibrosis markers and the nuclear translocation of NF-κB p65 in the kidney homogenates increased after exposure to MSNs. The in vitro study showed that MSNs cause cytotoxicity in NRK-52E cells and increased the expression of fibrosis markers. In addition, the NF-κB pathway could be induced, and inhibition of the NF-κB pathway could alleviate the fibrosis caused by MSNs. We conclude that inflammation is a major effector of the acute kidney toxicity induced by MSNs and results in renal interstitial fibrosis, which is mediated by the NF-κB signaling pathway.

Keywords: mesoporous silica nanoparticles (MSNs), acute kidney injury, renal interstitial fibrosis, NF-κB

Introduction

In the past 20 years, nanotechnology had undergone rapid development. Due to their favorable physical-chemical properties and biocompatibility, mesoporous silica nanoparticles (MSNs) have been widely used in numerous aspects, such as drug delivery, drug targeting, gene transfection, and cell tracking.[1–6] Due to the increasing applications of MSNs, it is important to study their adverse effects in vivo and explore their probable mechanism of toxicity. MSNs have been reported to enter the body through inhalation, injection, and dermal contact, resulting in a dose-dependent increase in the silica (Si) concentration in various organs, as observed in animal studies.[7–10] Most studies have focused on the toxicity in the liver and spleen, which are the major organs of the reticuloendothelial system,[11,12] and few studies have reported on injury in the kidney, which is the main excretory organ of MSNs.[13]

Currently, a review of the literature showed that Si nanoparticles can induce acute renal injury and that this toxicity is related to the size and characteristics of the nanoparticles.[14] However, few mechanisms underlying this nephrotoxicity have been mentioned.

Correspondence: Huang Zhiying
School of Pharmaceutical Sciences, 132 East Circle at University City, Guangzhou 510006, People's Republic of China
Tel +86 20 3994 3092
Fax +86 20 3994 3341
Email hzhiying@mail.sysu.edu.cn

submit your manuscript | www.dovepress.com
Dovepress
http://dx.doi.org/10.2147/IJN.S73538

Moreover, some in vitro studies have reported that several types of MSNs may cause renal cell damage and that the mechanism of injury is associated with the activation of oxidative stress and inflammation.[15,16] Nuclear factor kappa B (NF-κB) is a common type of transcription factor rapidly activated during inflammation. As an early transcription factor, there is no need to translate new proteins to activate NF-κB; therefore, it can react to the related stimulation as soon as possible.[17] The sustained over-activation of NF-κB can up-regulate the level of pro-inflammatory mediators/inflammatory mediators, induce the accumulation of infiltrating inflammatory cells, and result in the development of inflammation.[18,19] Because there is a large amount of NF-κB in various renal cells, the incidence of kidney disease is closely associated with the excessive activation of the NF-κB signaling pathway.[20] An increasing number of studies have demonstrated that the activation of NF-κB and the subsequent coordinated expression of gene products may play important roles in the pathogenesis of kidney diseases.

Therefore, to explore the potential toxicity of MSNs for its further biomedical applications, we set up the study described in the present paper to investigate its organ-specific toxicity in vivo after intraperitoneal administration in mice. In addition, the induction of cytotoxicity was evaluated in vitro as a function of dose and time of treatment, and the role of the NF-κB signaling pathway in the renal toxicity induced by MSNs was explored.

Materials and methods

Materials

Cetyltrimethylammonium bromide (CTAB) and tetraethyl orthosilicate (TEOS) were purchased from Sigma-Aldrich Co. (St Louis, MO, USA). Antibodies against NF-κB pathway were from Cell Signaling Technology, Inc. (Danvers, MA, USA). Antibody against ICAM-1 and FN were purchased from Santa Cruz Biotechnology Inc. (Dallas, TX, USA). BAY 11-7082 (NF-κB inhibitor) was from Beyotime Institute of Biotechnology (Haimen, People's Republic of China). Other chemicals were of analytical grade from commercial suppliers.

Synthesis of MSNs

MSNs were synthesized in alkaline media according to Lu et al report with some modifications according to our laboratory conditions.[21] TAB and TEOS were used as the template and silicon source, respectively. Briefly, in a three-necked flask 1.0 g CTAB and 0.28 g sodium hydroxide were dissolved in 480 mL water, and the resulting mixture was constantly stirred at 80°C until all CTAB was dissolved and the temperature became stable. Subsequently, 5 mL of TEOS was added dropwise to this solution, then the reaction solution was stirred for 2 hours (h). The solid product was collected by centrifugation and washed with water until the filtrate was neutral and then rinsed twice with alcohol before being dried at 60°C. Finally, the collected Si powder was calcined at 550°C for 8 h to completely eliminate the template. Fluorescein isothiocyanate (FITC)-labeled MSNs were used in a cellular uptake experiment.

MSNs' characterization

The morphology of MSNs was characterized by scanning electron microscopy (SEM) (JSM-6330F; JEOL, Tokyo, Japan), and the samples were gold-plated prior to imaging. The porous structure of the samples was analyzed by transmission electron micrographs (TEM) (JEM-1400; JEOL). Before examination, the Si materials were dispersed in 5% glucose and ultrasonicated for 10 minutes (min). The average size of the Si particles was determined by Zetasizer 3000HSA (Malvern Instruments, Malvern, UK) at 25°C.

Animals

Female BALB/C mice (6 weeks of age) were purchased from the Laboratory Animal Centre in Sun Yat-sen University, Guangzhou, People's Republic of China. All the mice were maintained in a specific pathogen-free animal room under controlled conditions at a temperature of 24°C±2°C, 55%±15% humidity, and a 12 h light/dark cycle. Food and water were provided ad libitum. The animals were allowed to acclimatize to the environment for 4 days before the experiment. All of the animal experimental procedures in this study were performed in accordance with the Sun Yat-sen University Guidelines for the Welfare of Animals (Approval No: IACUC-2013-0904).

The mice received a single intraperitoneal injection of a suspension of 150, 300 of 600 mg/kg MSNs in 5% glucose on day 1. The control mice were administered intraperitoneal injections of sterile 5% glucose. The mortality and clinical manifestations were recorded. After 2 days and 12 days, half of each group was euthanized, and the serum and organs were recovered.

TEM studies

The kidney tissues were dissected into 1 mm^3 pieces and immersed in fresh 5% glutaraldehyde in PBS overnight. The samples were treated at the Laboratory of Electron Microscopy of the Zhongshan School of Medicine of Sun

Yat-Sen University. The TEM images were observed under a transmission electron microscope (Tecnai G^2 spirit Twin; FEI Ltd., Hillsboro, OR, USA) operated at an accelerating voltage of 100 kV.

Histopathological examinations

A part of both kidneys was removed and immediately fixed in 4% paraformaldehyde in PBS (pH =7.4) at room temperature overnight. The histopathological tests were performed using standard laboratory procedures. The tissues were embedded in paraffin blocks, sectioned into 3 μm sections and mounted onto glass slides. After hematoxylin and eosin staining, the slides were observed and photographs were taken using an optical microscope (Leica DM5000B; Leica Microsystems, Wetzlar, Germany). The pathologist who performed all of the identifications and analyses of the pathology slides was blind to the treatment.

Masson's trichrome stain

The kidney paraffin sections were stained by Masson's trichrome stains. The slides were observed and photographs were taken using an optical microscope (Leica DM5000B; Leica Microsystems). The slides show red keratin and muscle fibers, blue or green collagen and bone, light red or pink cytoplasm, and dark brown to black cell nuclei. The pathologist who performed all of the identifications and pathological analyses of the slides was blind to the treatment.

Western blot analysis

To determine the protein expression of FN, TGF-β, ICAM-1, and NF-κB pathway proteins, part of the left kidney and the treated NRK-52E cells were subjected to Western blot analysis. Lysis buffer containing protease and phosphatase inhibitors was used. The samples (20 μg) were separated by 10% SDS-polyacrylamide gel electrophoresis and transferred to polyvinylidene difluoride membranes (EMD Millipore, Billerica, MA, USA). After being blocked in 5% non-fat milk in TBST (10 mM Tris-hydrochloric acid [HCl] [pH 8.0], 150 mM sodium chloride [NaCl], 0.1% Tween 20) for 1 h at room temperature, the membranes were incubated with the appropriate primary antibodies at 4°C overnight. The immunoblots were then incubated with a secondary antibody conjugated to horseradish peroxidase for 1 h at room temperature. The membranes were developed using an electrochemiluminescence (ECL) kit (Thermo Fisher Scientific, Waltham, MA, USA) according to the manufacturer's protocol. The signals were detected using a chemiluminescence detection system (Bio-Rad Laboratories Inc., Hercules, CA, USA). The density of the immunoreactive bands was analyzed using Quantity One-4.6.2 (Bio-Rad Laboratories Inc.).

MTT assay

NRK-52E cells were seeded in a 96-well plate at an initial density of 3.0×10^3 cells/well. Twenty-four hours after seeding, the cells were treated with control (Dulbecco's Modified Eagle's Medium [DMEM]) or different concentrations of MSNs for 3 and 24 h. Following treatment, the cells were incubated with 5 mg/mL MTT tetrazolium (20 μL/well) for 4 h at 37°C. The resulting violet formazan precipitate was solubilized with dimethyl sulfoxide (DMSO) (150 μL). After gently shaking at 37°C for 10 min, the absorbance of the dissolved formazan grains within the cells was measured at 570 nm using a microplate reader (Thermo Multiskan Ascent 354; Thermo Fisher Scientific).

Lactate dehydrogenase (LDH) leakage assay

NRK-52E cells were seeded in 24-well plates at a density of 4×10^4 cells/well and treated with different concentrations of MSNs for 3 and 24 h. The cell viability was then assessed by determining the release of LDH from the cells using an LDH Detection Kit (Nanjing Jiancheng Bioengineering Institute, Nanjing, People's Republic of China) according to the manufacturer's instructions. The enzyme activity was expressed as the percentage of extracellular LDH activity relative to the total LDH activity.

Cellular uptake

The uptake of MSNs by NRK-52E cells was visualized by confocal microscopy. The cells were grown on 35 mm glass-bottom microwell dishes (Nest, Wuxi, People's Republic of China) and incubated for 0, 15, 30, 180 min with 100 μg/mL FITC-labeled MSNs. The cell nuclei and cytoskeleton were stained with 2.5 μM 4′,6-diamidino-2-phenylindole (DAPI) and 2.5 μM Phalloidin-tetramethyl-rhodamine (TRITC), respectively, for 20 min. Fluorescent images of the cells were obtained under a confocal laser scanning microscope LSM710 (Carl Zeiss Meditec AG, Jena, Germany).

Measurement of levels of TNF-α, IL-β, and IL-6

NRK-52E cells were seeded in 24-well black plates at a density of 4×10^4 cells/well, and then exposed to different concentrations of MSNs, LPS, and BAY 11-7082. Following

treatment, 100 μL supernatant and cell lysate were collected. TNF-α, IL-β, and IL-6 levels were detected by rat TNF-α, IL-β, and IL-6 enzyme-linked immunosorbent assay (ELISA) kits (Dakewe Biotech, Guangdong, People's Republic of China) according to the procedures provided by the manufacturer.

Immunofluorescence staining

After treatment, NRK-52E cells were fixed with 10% paraformaldehyde in PBS (15 min, RT), blocked for 30 min with 10% normal goat serum in PBS containing 0.3% triton, and incubated with primary antibodies diluted in blocking buffer (NF-κB p65, 1:50) for 1 h at room temperature. After washing with PBS, the cells were incubated with Alexa Fluor 488-labeled goat anti-rabbit immunoglobulin G (Beyotime Institute of Biotechnology) (diluted 1:1,000 in blocking buffer) for 1 h and washed with PBS. Coverslips were mounted in Prolong Gold antifade reagent with DAPI and inspected with a confocal laser scanning microscope LSM710 (Carl Zeiss Meditec AG).

Statistical analysis

The SPSS v16.0 software (SPSS Inc., Chicago, IL, USA) was used for the statistical analyses. The values are expressed as the means ± standard error of the mean. The intergroup differences were assessed using one-way analysis of variance (ANOVA) followed by Dunnett's method. The differences between groups were determined using two-way ANOVA followed by the Bonferroni correction post hoc analysis for multiple comparison procedure. The level of significance was set to $P<0.05$.

Results

Preparation and characterization of MSNs

The SEM image (Figure 1A) and the TEM image (Figure 1B) indicate that the morphology of MSNs is round (as spherical) with a homogeneous pore structure inside. The average diameter of the MSNs was found to be 198.2±21.8 nm in 5% glucose solution (Figure 1C), with the particle dispersion index of 0.146±0.067. These data demonstrate that, under our experimental conditions, the suspended MSNs were found in their individual form with a uniform size distribution. The MSNs were sterilized by UV irradiation for 1 h, suspended in sterile 5% glucose solution and sonicated for 30 min before being loaded into 1 mL syringes under sterile conditions.

Acute kidney injury (AKI) of MSNs in Balb/c mice

To explore the acute injury induced by MSNs, 40 mice were randomly assigned to four groups and exposed to nanoparticles at dosages of 150, 300, and 600 mg/kg. The mice received a single intraperitoneal injection of the MSNs suspended in 5% glucose. When exposed to the 600 mg/kg dosage, three of the ten mice died after 2 days. Moreover, weight loss could be observed in all of the treated groups during the first 3 days after injection. After 2 days and 12 days, half of the animals in each group were euthanized, and the serum and organs were recovered. After 2 days, the morphology of the kidney in the high-dose group was larger and exhibited edematous, and the color was grey and bloodless, and after 12 days, the kidney shape narrowed, resulting in an uneven appearance (Figure 2A). In the middle-dose group, we found similar but milder findings, whereas the low-dose group showed no anomalies. Because the relative liver weight of the control group exhibited a marked difference between 2 days and 12 days after administration, we could not make a comparison between them. A statistically significant change was observed in the 600 mg/kg dose group compared with the control after 12 days (Figure 2B, left). In contrast, the relative kidney weight of the control group presented no significant difference between 2 days and 12 days after administration; thus, an among-groups comparison could be made. After 2 days, the relative kidney weights of the middle- and high-dose group presented a significant increase compared with the control, whereas after 12 days, the relative kidney weights decreased and showed no significant difference compared with the control, although a significant difference was found with the corresponding group in the 2 days comparisons, respectively (Figure 2B, right). Blood biochemical parameters that reflect the hepatic and nephritic functions were investigated. The alanine aminotransferase level increased after MSN administration at a dose of 600 mg/kg after 2 days, whereas no increase was observed with the same dose after convalescence. Similarly, the aspartate aminotransferase level increased with the MSN administration at doses of 300 and 600 mg/kg after 2 days and then decreased after convalescence. The blood urea nitrogen level presented a significant increase 2 days after the administration of MSNs at doses of 300 and 600 mg/kg, and even after 10 days convalescence, the level was approximately two-fold greater than the control value. In contrast, the injection of MSNs at 300 and 600 mg/kg may slightly decrease the creatinine level after 2 days. However, after the recovery

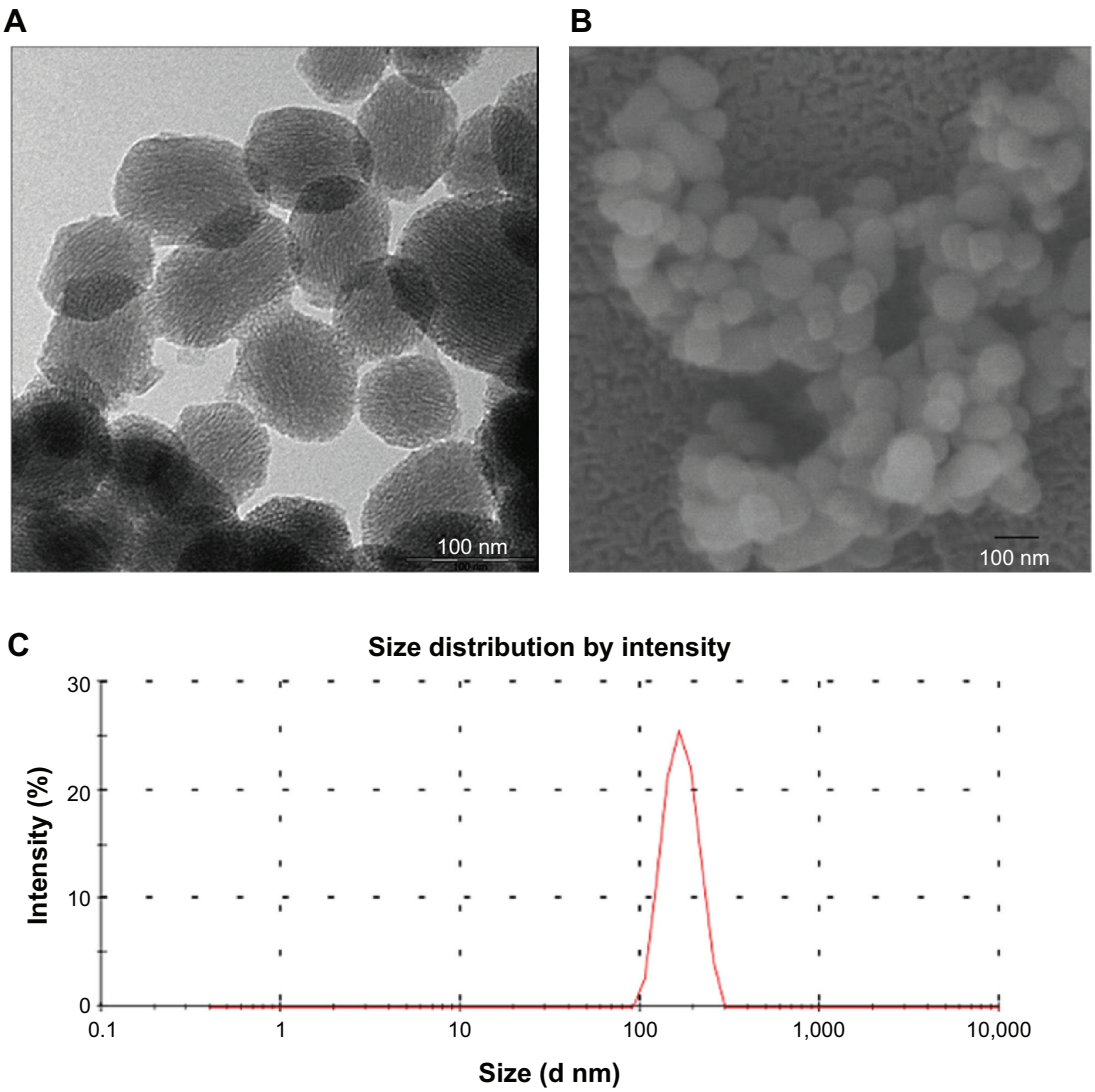

Figure 1 Characterization of MSNs.
Notes: Size distribution of MSNs following dispersion in 5% glucose. Particle size distribution evaluated from the corresponding SEM (**A**) and TEM micrographs (**B**). Mean particle size (**C**) of the ordered mesoporous silica. The scale is indicated at the right lower corner. The average diameter of the MSNs was found to be 198.2±21.8 nm in 5% glucose solution, with the particle dispersion index of 0.146±0.067.
Abbreviations: MSNs, mesoporous silica nanoparticles; SEM, scanning electron microscopy; TEM, transmission electron micrographs.

period, the level showed a statistically significant increase in the 300 mg/kg group compared with the level observed after 2 days. Besides, the level obtained with the dose of 600 mg/kg was significantly lower than that observed in the control. As shown in Figure 2D, the TEM images revealed that the absorbed MSNs appeared to be monodispersed and were rounded in shape in the kidney.

Histopathological examination of kidney tissues

The histopathological evaluations of kidney tissues were conducted under light microscopy with hematoxylin and eosin staining, as depicted in Figures 3A and B. After 2 days, no abnormal histological characteristics were observed in the kidney tissues of the 150 mg/kg group compared with the control. However, in the 300 and 600 mg/kg dose group, cortical tubular necrosis and some tubular eosinophil degeneration were observed (Figures 3A and S1). After 12 days, mild focal interstitial fibrosis and slight tubular epithelial cell necrosis were observed in one mouse in the 150 mg/kg group. In the 300 and 600 mg/kg dose group, renal interstitial fibrosis and a small amount of lymphocytic infiltration were found, and some tubular necrosis, glomerular basement membrane thickening, and renal tubular regeneration were also observed (Figures 3B and S2).

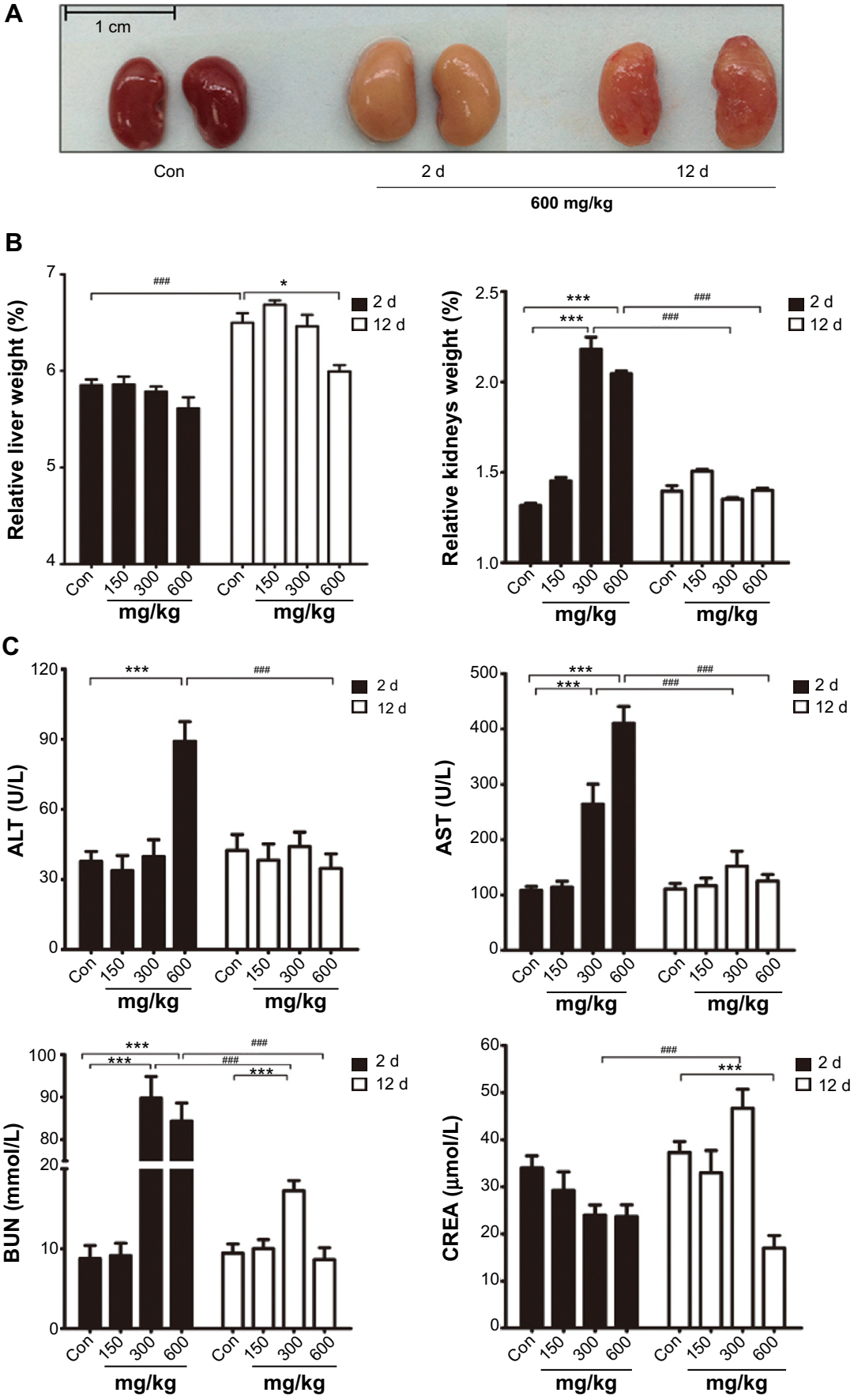

Figure 2 (*Continued*)

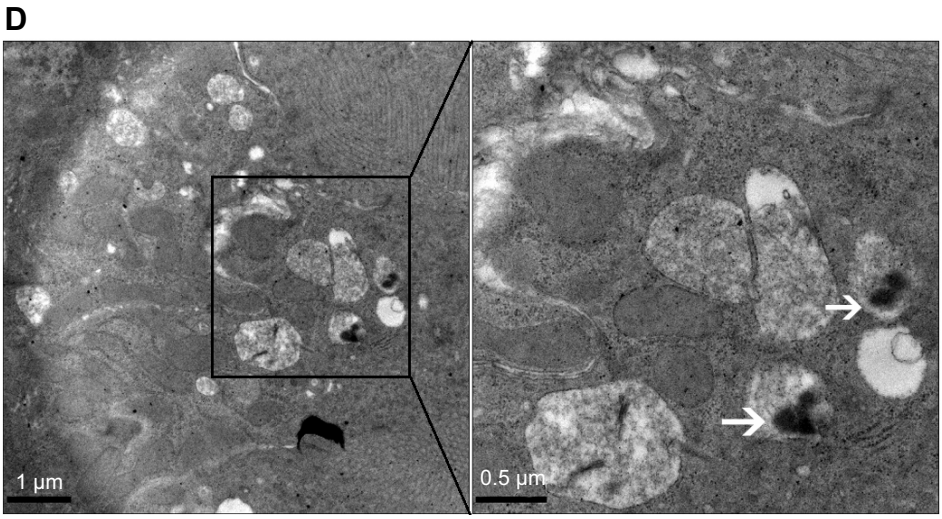

Figure 2 Effects of MSNs in Balb/c mice.
Notes: The kidney appearances of the treated mice: con, 600 mg/kg (for 2 days) and 600 mg/kg (for 12 days) (**A**). All of the mice were treated with a single intraperitoneal injection. Relative liver and kidney weights of the treated mice (**B**). Biochemical analysis of aspartate aminotransferase (AST), alanine aminotransferase (ALT), blood urea nitrogen (BUN), and creatinine (CREA) (**C**). The TEM photos of the renal tubular epithelial cell after treatment with 300 mg/kg MSNs for 2 days were enlarged 23,000- and 46,000-fold; MSNs indicated by arrows (**D**). The data are expressed as the means ± standard error of the mean (n=5). $^{*}P<0.05$ and $^{***}P<0.001$ versus intragroup con; $^{\#}P<0.05$ and $^{\#\#\#}P<0.001$ among groups.
Abbreviations: MSNs, mesoporous silica nanoparticles; SEM, scanning electron microscopy; TEM, transmission electron micrographs; d, day(s); con, control.

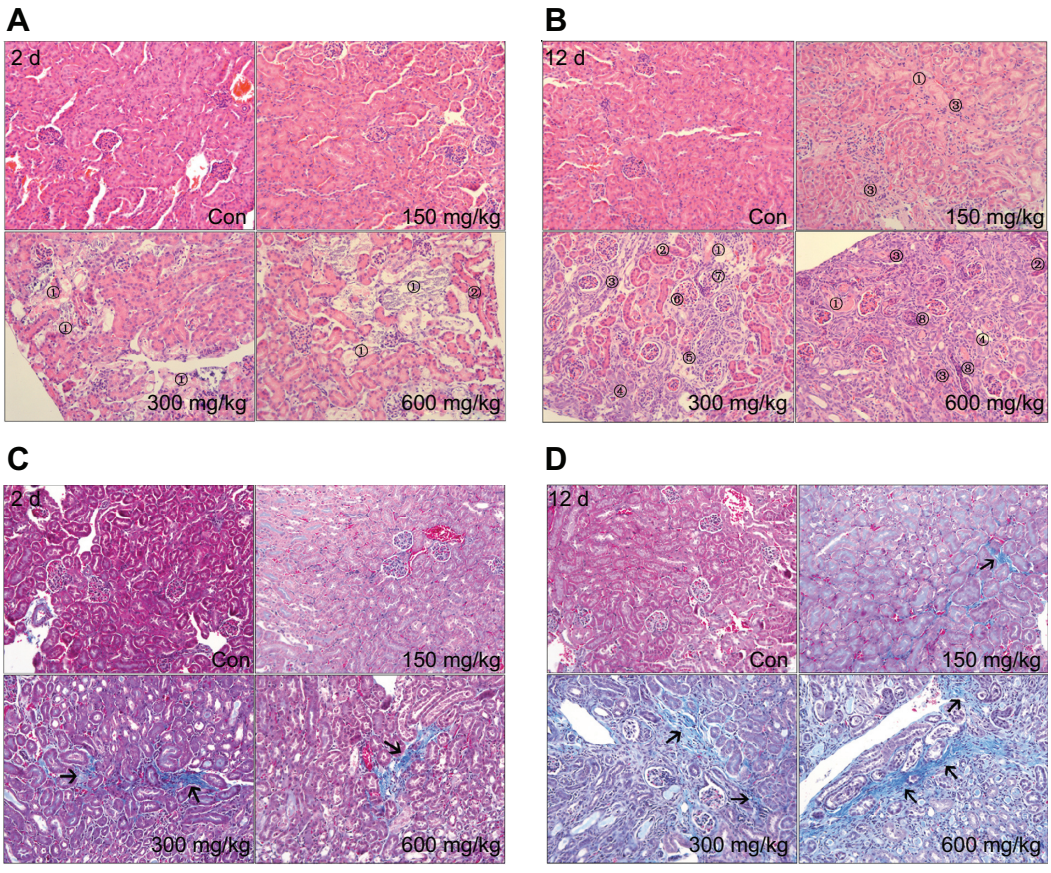

Figure 3 Pathologic changes induced by MSNs in Balb/c mice.
Notes: Kidney injury and renal interstitial fibrosis in the control and MSN-treated groups after 2 days and 12 days were detected by hematoxylin and eosin (**A** and **B**) and Masson staining (**C** and **D**) (magnification 200×), respectively. Because various lesions were observed, numbers were used to indicate the local lesions. 1) Tubular necrosis, 2) tubular eosinophil degeneration, 3) renal interstitial fibrosis, 4) tubular regeneration, 5) renal interstitial lymphocytic infiltration, 6) mesangial cells proliferation, 7) glomerular basement membrane thickening, 8) cellular casts in tubules. In (**C** and **D**), the arrows indicate the collagen fiber accumulation in the kidney, which was stained blue with Masson staining.
Abbreviations: MSNs, mesoporous silica nanoparticles; d, day(s); con, control.

Collagen fiber deposition was assessed using Masson's trichrome staining in the histological sections of the kidney (Figures 3C and D and S3-4). In the middle and high-dose group, collagen fiber accumulation with blue staining was observed after 2 days (Figures 3C and S3). After 12 days, the interstitial fibrotic area of the middle- and high-dose groups was increased compared with that observed after 2 days (Figures 3C and S3).

Fibrosis and inflammation induced by MSNs in the kidney

In the kidney, FN is one of the major forms of ECM proteins and is produced mainly by fibroblasts; TGF-β and ICAM-1 are considered markers of fibrosis. As shown in Figure 4A, the expression levels of FN, TGF-β, and ICAM-1 significantly increased in response to the doses of 300 mg/kg and 600 mg/kg after both 2 days and 12 days compared with the control. Furthermore, the nuclear translocation of p65 was induced in the middle- and high-dose groups after 2 and 12 days, and this difference was significant compared with the control.

Cytotoxicity and cellular uptake of MSNs in NRK-52E

The MSNs-induced nephrotoxicity in vitro was examined using NRK-52E cells treated with various concentrations of MSNs for 3 and 24 h; the cell viability in these studies was measured using the MTT assay. As shown in Figure 5A, MSNs reduced NRK-52E cell viability in a dose- and time-dependent manner. After 24 h of exposure, the MSNs produced severe cytotoxicity in NRK-52E cells with an IC_{50} value of 849.10±50.16 μg/mL. We also measured the cytotoxic effect of MSNs by measuring the LDH leakage, which is a biomarker that indicates the integrity of the cell membrane. Twenty-four hour incubation with various concentrations of MSNs (from 200 to 800 μg/mL) markedly induced the release of LDH (Figure 5B). To directly observe the uptake of MSNs by NRK-52E, we used confocal microscopy to visualize the distribution of MSNs at 15, 30, and 180 min. A few green dots were observed inside the membrane at 15 min, more green dots translocated from the membrane to the cytoplasm at 30 min, and the cytoplasm was full of green dots at 180 min (Figures 5C and S5–8). This result indicates that the uptake of MSNs by NRK-52E occurs in a time-dependent manner and shows saturation at approximately 180 min.

Fibrosis and inflammation induced by MSNs in NRK-52E

To verify whether MSNs can also induce fibrosis and inflammation in vitro, we examined the expression of FN, TGF-β, and ICAM-1 by Western blotting. The results showed that MSNs could significantly induce the expression of the above-mentioned proteins (Figure 6A). The Western blot analysis showed that treatment with 50–400 μg/mL MSNs for 24 h increases the protein level in a dose-dependent manner and a slight decrease was observed with the dose of 800 μg/mL. Moreover, in the time course, the protein level started to increase at 6 h, reached the peak between 9 and 12 h, and declined thereafter. Because TGF-β and ICAM-1 are related to the development of inflammation and NF-κB signaling is a classical inflammation-dependent pathway, the IκBα level was examined. As shown in Figure 6B, the IκBα level significantly decreased in a dose- and time-dependent manner. Incubation with 200 μg/mL MSNs for 24 h or with 400 μg/mL MSNs for 9 h resulted in significant reduction compared with the control, and incubation with a higher dose or for a longer duration resulted in a greater reduction in the level of IκBα.

Activation of the NF-κB signaling pathway by MSNs in NRK-52E

To further explore the underlying molecular mechanism of the effects induced by MSNs on FN, TGF-β, and ICAM-1 expression, the activation of NF-κB was examined. Because the activation of NF-κB signaling is a rapid response, the protein levels were examined from 5 to 180 min. As shown in Figure 7C, incubation with the MSNs results in a marked activation of phosphorylated IKKα/β, phosphorylated IκBα, and phosphorylated p65 at 400 μg/mL for 5 min, and the levels of these proteins declined thereafter. Incubation with the MSNs for 30 min and longer resulted in a secondary activation of phosphorylated IKKα/β, phosphorylated IκBα, and phosphorylated p65. During the treatment, the total IKKα and p65 contents were not altered, whereas the total IκBα content presented a significant decrease after an hour of incubation. Moreover, treatment with 50–400 μg/mL MSNs for 5 min could activate phosphorylated IKKα/β, phosphorylated IκBα, and phosphorylated p65 in a dose-dependent manner, whereas incubation with 800 μg/mL for the same duration could not activate the above-mentioned proteins. Among the various dose treatments, the total IKKα and p65 contents were not altered, but the total IκBα decreased with the dosage of 800 μg/mL. Because NF-κB p65 nuclear translocation is a key event in the activation of this pathway, we also examined NF-κB p65 nuclear accumulation to investigate the effect of MSNs on NF-κB activation. As shown in Figure 7A, the NF-κB p65 nuclear levels started to increase at 5 min, reached the peak values at approximately 15 to 30 min, and declined thereafter.

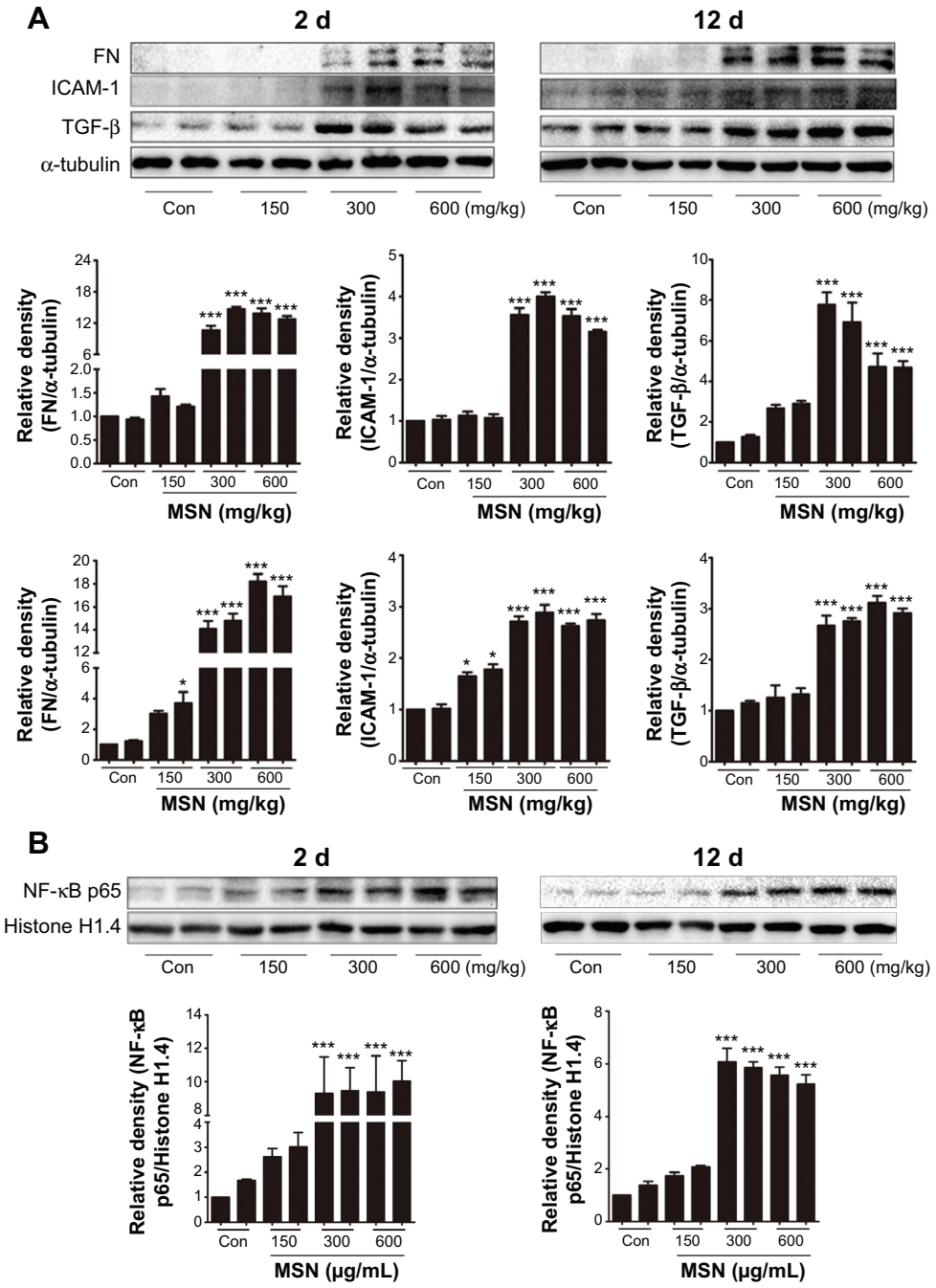

Figure 4 MSNs increased kidney fibrosis in Balb/c mice 2 days and 12 days after injection.
Notes: The proteins (20 μg) of the total lysates extracted from the left kidney were subjected to SDS-PAGE followed by Western blot with the indicated antibodies (**A** and **B**). α-Tubulin was used as the loading control. The blots were then quantified by densitometry. The data are expressed as the means ± standard error of the mean. The results are representative of three independent experiments. (*$P<0.05$ and ***$P<0.001$ versus con intragroup, ANOVA).
Abbreviations: MSNs, mesoporous silica nanoparticles; d, day(s); ANOVA, analysis of variance; NF-κB, nuclear factor kappaa B; con, control.

Moreover, treatment with various doses of MSNs for 15 min increased the nuclear levels of NF-κB p65 in a dose-dependent manner, and the highest levels were obtained with 400 μg/mL. LPS, which is a well-known NF-κB activator, was utilized as a positive control.

The activation of NF-κB signaling in response to MSNs was also evident from the induction of several NF-κB-target genes. As shown in Figure 7E and F, the expression of TNF-α, IL-1β, and IL-6 was detected. MSNs showed a significant development of inflammation by increasing the inflammatory cytokines including TNF-α and IL-1β production and release, in both dose- and time-dependent manner. However, there was not a significant increase of IL-6 production and release by MSNs. This findings may

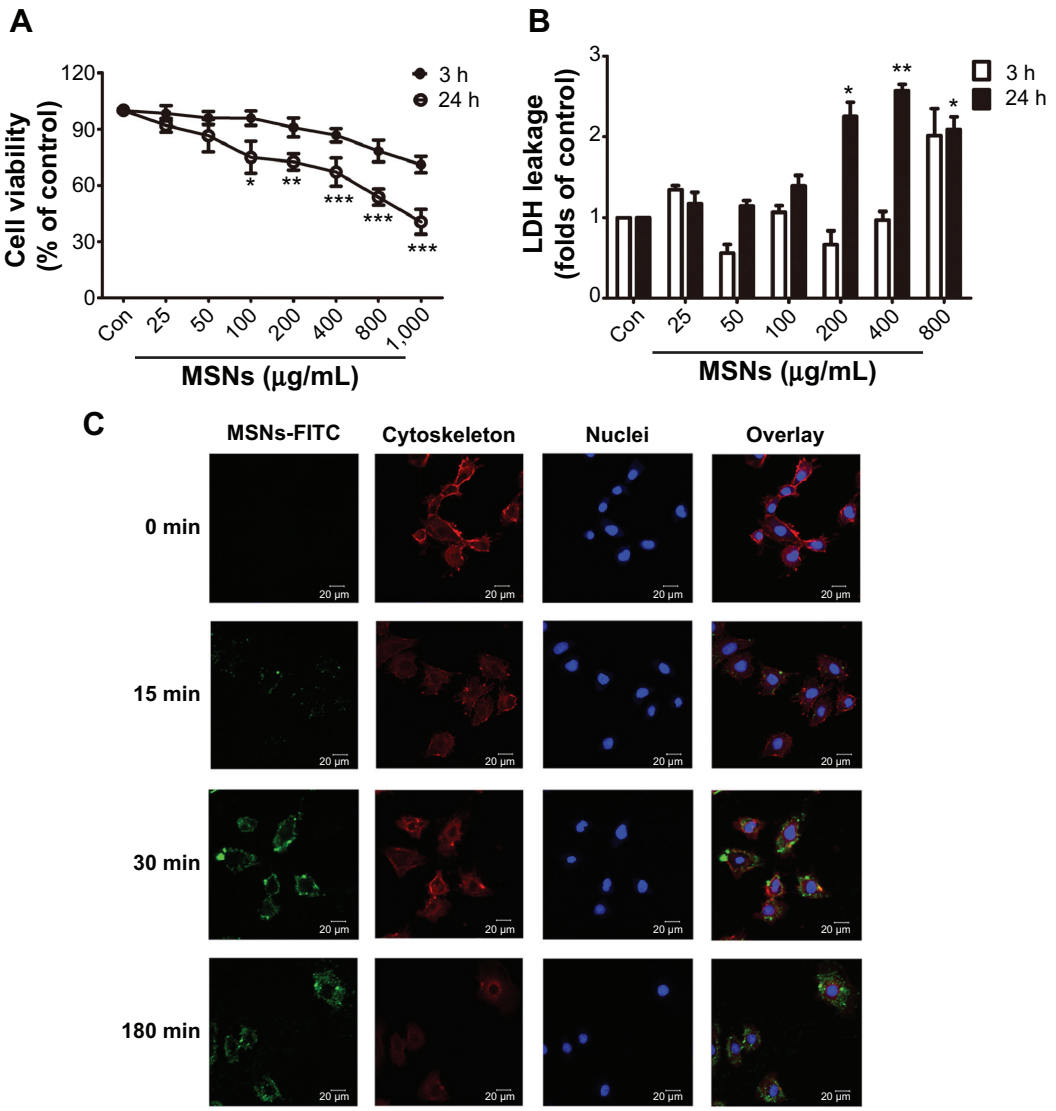

Figure 5 Effects of MSNs on NRK-52E cells.

Notes: (**A**) NRK-52E cells were treated with MSNs at various concentrations for 3 h and 24 h. The cell viability was determined by an MTT assay. The viability of the cells that were not treated with MSNs is defined as 100%. (**B**) For the LDH release assay, NRK-52E cells were treated as in (**A**), and the conditional medium was harvested for LDH assay. The data are expressed as the means ± standard error of the mean. The results are representative of three independent experiments. (*$P<0.05$, **$P<0.01$, and ***$P<0.001$ versus con, ANOVA). (**C**) The uptake of MSNs by NRK-52E cells was detected at 0, 15, 30, and 180 min. MSNs were stained green due to their labeling with FITC, the cytoskeleton presented red staining due to Phalloidin-TRITC, and the nuclei were stained blue due to DAPI staining.

Abbreviations: MSNs, mesoporous silica nanoparticles; NRK, normal rat kidney; h, hour(s); min, minutes; LDH, lactate dehydrogenase; ANOVA, analysis of variance; FITC, fluorescein isothiocyanate; TRITC, tetramethylrhodamine; DAPI, 4′,6-diamidino-2-phenylindole; con, control.

suggest that the activation of NF-κB-target genes is an alternative.

Fibrosis and inflammation alleviation induced by MSNs through NF-κB pathway inhibition in NRK-52E

To investigate whether the fibrosis and inflammation induced by MSNs in NRK-52E cells is attributed to activation of the NF-κB pathway, we inhibited NF-κB and then examined the expression of FN, TGF-β, and ICAM-1 by Western blot. First, we examined the inhibitory effect of BAY 11-7082, which is regarded as a common NF-κB inhibitor, could down-regulated the LPS-induced inflammation, by western blot and confocal microscopy. Here, LPS was utilized as a positive control. As shown in Figure 8A, pre-treatment with BAY 11-7082 followed by co-incubation with MSNs resulted in a reduction in NF-κB p65 nuclear translocation to levels equal to those observed in the control, and this reduction was significant compared with the MSN-treated group. As shown in Figure 8B, the

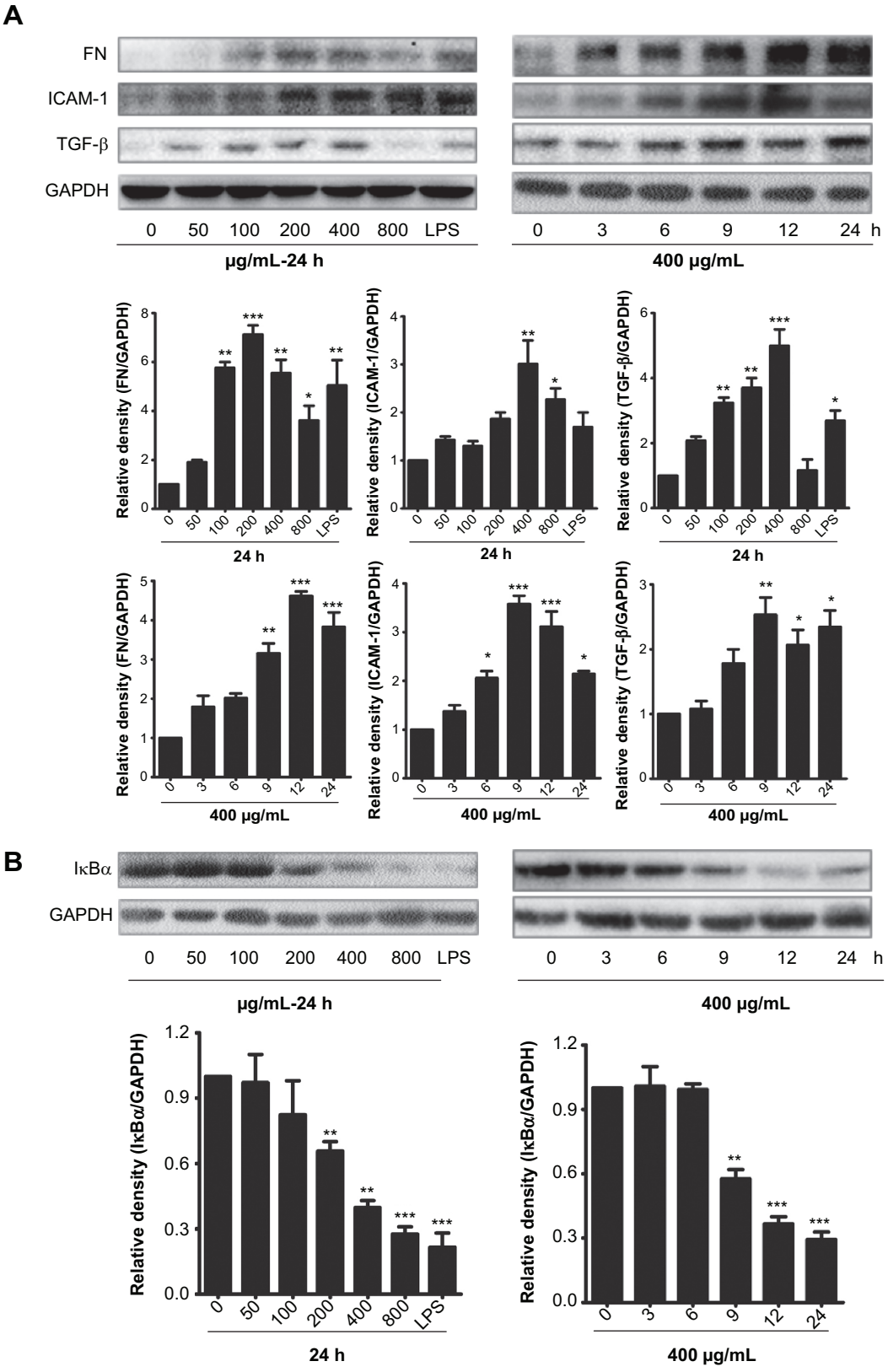

Figure 6 Fibrosis and inflammation induced by MSNs in NRK-52E cells.

Notes: Fibrosis (**A**) and inflammation (**B**) induced by MSNs in NRK-52E cells. NRK-52E cells were treated with the indicated concentration of MSNs for 24 h and treated with 400 μg/mL MSNs for the indicated times. The proteins (20 μg) of the total lysates extracted from the NRK-52E cells were subjected to SDS-PAGE followed by Western blot with the indicated antibodies. GAPDH was used as the loading control. The blots were then quantified by densitometry. The data are expressed as the means ± standard error of the mean. The results are representative of three independent experiments. (*$P<0.05$, **$P<0.01$, and ***$P<0.001$ versus con, ANOVA).

Abbreviations: MSNs, mesoporous silica nanoparticles; NRK, normal rat kidney; h, hour(s); ANOVA, analysis of variance; con, control; LPS, Lipopolysaccharides.

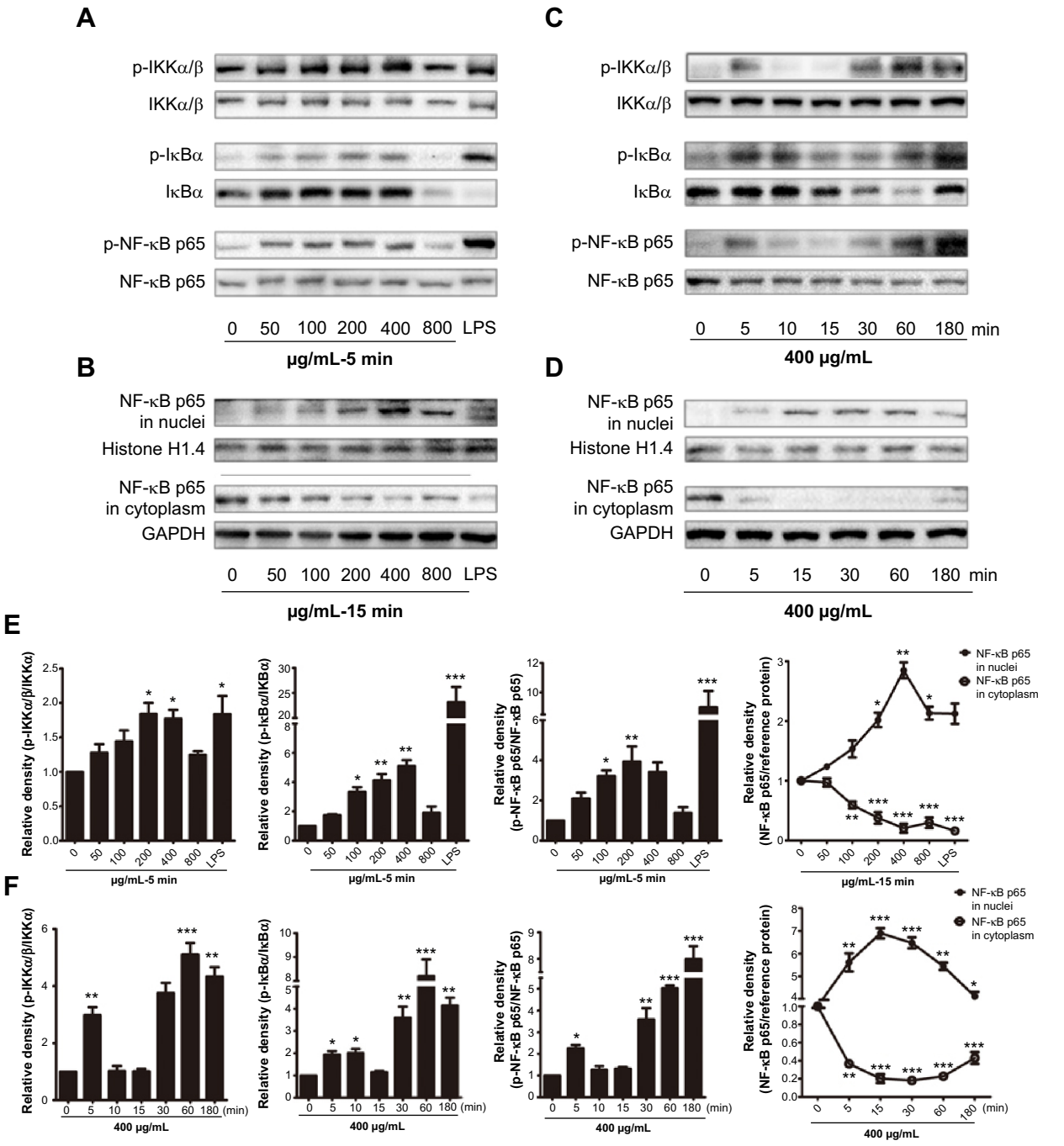

Figure 7 Effects of MSNs on the activation of the NF-κB signaling pathway.

Notes: NRK-52E cells were treated with the indicated concentrations of MSNs for 5 min (**A**),15 min (**B**), and 30 min (**E**); or treated with 400 μg/mL MSNs for the indicated time (**C**, **D** and **F**). The proteins (20 μg) of the total lysates and the nuclear (15 μg) and cytoplasm proteins (15 μg) extracted from NRK-52E cells were subjected to 10% SDS-PAGE followed by Western blot with the indicated antibodies. NRK-52E cells treated with 2 μg/mL LPS served as the positive control. Histone H1.4 and GAPDH were used as the loading controls for the nuclear and cytoplasmic proteins, respectively. The blots were then quantified by densitometry. TNF-α, IL-1β, and IL-6 production was assessed using ELISA assay (**E** and **F**). The data are presented as the means ± standard error of the mean from three independent experiments. (*$P<0.05$, **$P<0.01$, and ***$P<0.001$ versus con, ANOVA).

Abbreviations: MSNs, mesoporous silica nanoparticles; NF-κB, nuclear factor kappa B; NRK, normal rat kidney; min, minutes; ANOVA, analysis of variance; ELISA, enzyme-linked immunosorbent assay; con, control; LPS, Lipopolysaccharides.

immunofluorescence staining of NF-κB p65 showed green staining mainly in the nuclei of the MSN- and LPS-treated groups, whereas the staining was dispersed in the cytoplasm of the control and NF-κB-inhibited groups. In addition, BAY 11-7082 significantly down-regulated the MSNs-induced inflammatory factors including TNF-α, IL-1β, and IL-6 production and release, as shown in Figure 8D. Then, we examined the expression of fibrosis- and inflammation-related

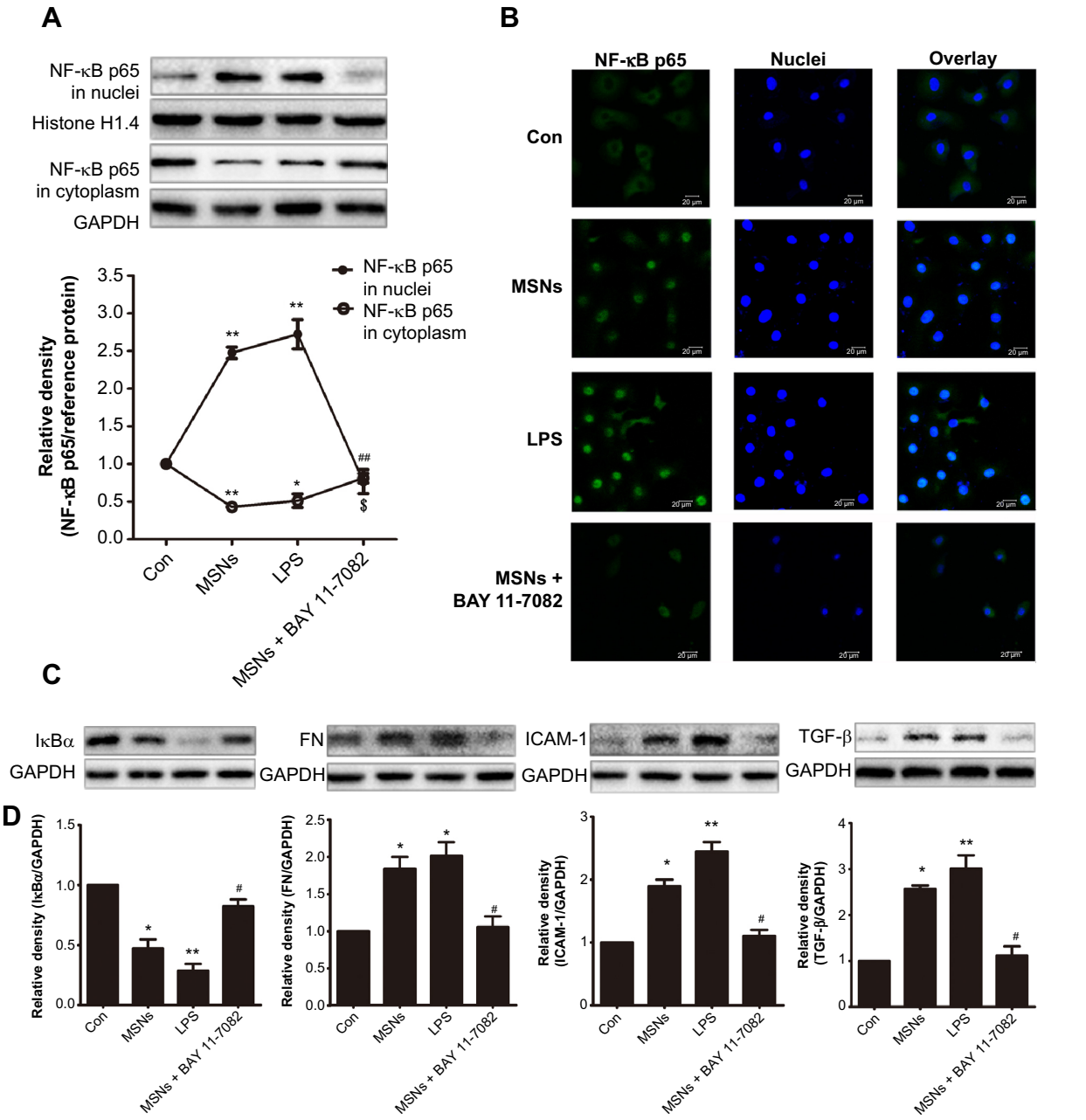

Figure 8 Reduction of the fibrosis by MSNs on NRK-52E cells through inhibition of the NF-κB pathway.

Notes: The changes in the protein expression (**A**) and immunofluorescence staining (**B**) of NF-κB p65 in the nuclei and cytoplasm were evaluated through Western blot analysis and confocal microscopy. MSNs: 400 μg/mL MSNs for 30 min; LPS: 2 μg/mL LPS for 30 min; MSNs + BAY 11-7082: pre-treatment with 3 μM BAY 11-7082 for 1 h followed by treatment with MSNs for 30 min. The fibrosis reduction was measured by Western blot with the indicated antibodies (**C**). MSNs: 400 μg/mL MSNs for 24 h; LPS: 2 μg/mL LPS for 24 h; MSNs + BAY 11-7082: pre-treatment with 3 μM BAY 11-7082 for 2 h followed by treatment with MSNs for 24 h. Histone H1.4 and GAPDH were used as the loading control for the nuclear and cytoplasmic proteins, respectively. TNF-α, IL-1β, and IL-6 production (**D**) was assessed using ELISA assay. MSNs: 400 μg/mL MSNs for 2 h; LPS: 2 μg/mL LPS for 30 min; MSNs + BAY 11-7082: pre-treatment with 3 μM BAY 11-7082 for 1 h followed by treatment with MSNs for 2 h. The data are expressed as the means ± standard error of the mean. The results are representative of three independent experiments. (*$P<0.05$, and **$P<0.01$ versus con, #$P<0.05$, and ##$P<0.01$ versus MSNs, ANOVA).

Abbreviations: MSNs, mesoporous silica nanoparticles; NF-κB, nuclear factor kappa B; NRK, normal rat kidney; min, minutes; h, hour(s); ELISA, enzyme-linked immunosorbent assay; ANOVA, analysis of variance; con, control; LPS, Lipopolysaccharides.

proteins by Western blot. As shown in Figure 8C, pre-treatment with BAY 11-7082 followed by co-incubation with MSNs increased the expression of IκBα and decreased the expression levels of FN, TGF-β, and ICAM-1, and these differences were statistically significant.

Discussion

MSNs are emerging as a new and promising type of nanoparticle for drug delivery systems due to their special structures.[25–27] However, the concerns associated with the biocompatibility caused by MSNs have also increased,[28,29]

and standardized procedures for the evaluation of their toxicity have not been defined. The risk of human exposure is rapidly increasing and reliable toxicity test systems are urgently needed. Toxicity assessment is critical for the development of nanoparticle-based drugs, because of nanoparticle-enhanced biological reactivity.[30,31] This study was undertaken to investigate the potential toxicity of newly synthesized MSNs in biomedical applications. In this study, we focused on two aims: 1) to observe the injury to the kidney after a single intraperitoneal injection, and 2) to explore the role of the NF-κB inflammatory signaling pathway in the induced nephrotoxicity and renal tubular-interstitial fibrosis (TIF) as a potential mechanism.

As well known, investigation of the acute toxicity is the first step in the toxicological investigations of an unknown substance. And it is widely accepted that the purpose of conducting an acute toxicity study is to reflect the accumulated toxicity and targeted organs in vivo, by maximizing the doses of exposure, via a single high-dose injection. The index of the acute toxicity is the LD_{50}. The LD_{50} was recognized and justified of being the best parameter.[32] In our preliminary experiments, the LD_{50} was 800 mg/kg, and the 95% confidence interval was 609.1–1,130 mg/kg. (Table S1). Besides, we found no published studies that explicitly followed the preclinical safety pharmacology guidelines of regulatory agencies such as the US Food and Drug Administration (FDA), International Conference on Harmonization and the European Medicines Agency which recommend assessing toxicity at least ten to 100 times higher than the projected therapeutic dose.[33–36] So we used the dose of 150, 300, and 600 mg/kg in our acute toxicity study. Thus, as a part of the preclinical in vivo safety pharmacology evaluation, here, we report dose response, expanded acute toxicology, and nephritic safety pharmacology assessment of MSNs in mice.[37] This study was carried out to add scientific data in regard to the use of MSNs in nanomedicine.

To investigate the hypothesis, we first performed in vivo studies. In recent years, an increasing number of studies have shown that AKI and chronic kidney disease are significantly correlated.[38,39] According to the histopathology study, severe renal tubular epithelial cell (RTEC) damage is the first step in the development from AKI to chronic kidney disease. The pro-fibrogenic cytokines secreted by damaged tubular cells can activate fibroblasts, leading to renal TIF. In our preliminary studies, most of the administered nanoparticles have been reported to be excreted from the kidney or hepatobiliary pathways within 15 days.[40,41] To date, many studies have focused on the interaction and toxicity in the liver,[42–44] but few nephrotoxicity mechanisms have been reported. We found that a single intraperitoneal injection with a high dose led to a severe and selective renal toxicity. These findings arouse our interest, and we designed in vitro and in vivo research to explore the potential mechanisms of the renal toxicity. Then, in our formal study, selective AKI was observed 2 days after exposure. Morphological, relative weight and biochemical changes were observed in our study during the early stage of MSN exposure (Figure 2), which necessarily indicated renal functional damage. The pathological changes indicated that the kidney tubules were the most important locus of the observed injury (Figures 3A and S1).

All progressive renal diseases are the consequence of a process of destructive fibrosis, and RTEC damage is the source of TIF. Therefore, in the present study, we chose to use the rat RTEC line NRK-52E as a model to conduct MTT and LDH leakage analyses in order to determine whether the effect of MSNs on NRK-52E cell viability is cytotoxic in a dose- and time-dependent manner (Figure 5A and B). Because the cytotoxicity induced by MSNs may be related to their uptake by cells,[45,46] we observed that MSNs are not only absorbed by NRK-52E cells in a time-dependent manner but also localized predominantly in RTECs (Figures 5C, 2D, and S5–8. These findings provide evidence to corroborate the hypothesis.

From the pathophysiology, TIF could be divided into four arbitrary phases.[38] The first is related to cellular activation and injury. The tubules are activated, and myofibroblasts/activated fibroblasts populate the interstitium. The second is the fibrogenic signaling phase, in which several growth factors and cytokines, such as TGF-β and ICAM-1 (CD54), are implicated. The third is the fibrogenic phase, in which ECM proteins, including collagens I, III, and FN, accumulate. The fourth is the phase of renal destruction. Thus, we chose TGF-β, ICAM-1, and FN as fibrosis markers to investigate the TIF 2 days after exposure. Treatment with MSNs significantly increased the expression of FN, TGF-β, and ICAM-1 in the kidney homogenate compared with the control (Figure 4A left). Moreover, a slight collagen fiber accumulation was observed (Figures 3C and S3). These findings indicate that MSNs induce kidney injury and fibrosis 2 days after exposure. The inflammation and fibrosis induced by occupational exposure to quartz, mineral dust particles, and asbestos have been observed in the lung.[7,47,48] However, to the best of our knowledge, no in vivo study has ever investigated the renal fibrosis induced by MSNs.

To investigate the reversibility of the nephrotoxicity and the progress of TIF, we designed a convalescence study 12

days after exposure. The renal function improved to some extent after convalescence (Figure 2B), but the TIF process was further developed due to greater collagen fiber accumulation (Figures 3D and S4), the persistent up-regulation of FN, TGF-β, and ICAM-1 expression (Figure 4A), and the renal interstitial fibrosis observed by hematoxylin and eosin staining 12 days after exposure (Figures 3B and S2). The findings observed from 2 days to 12 days after exposure showed that a single intraperitoneal administration of MSNs first causes AKI in mice, induces the release of pro-fibrotic signals, and then results in TIF. We observed similar findings in vitro: MSNs could also increase the expression of FN, TGF-β, and ICAM-1 in a dose- and time-dependent manner (Figure 6). After convalescence, the necrotic renal tubular cells exhibited regeneration, and the renal function recovered to some extent; however, the AKI and progression of TIF was further developed, indicating that the nephrotoxicity induced by MSNs could not be reversed after 12 days.

Some recent studies have shown that a severe inflammatory response induced by MSNs is a common initial step in their toxicity in vivo and in vitro.[49] Some studies have identified oxidative stress-related changes in gene expression and cell signaling pathways as the main traits of nanoparticle-induced cytotoxicity.[50] The NF-κB pathway plays an important role in both inflammatory and oxidative stress. In contrast, the activation of the NF-κB inflammatory pathway plays an important role in the TIF process.[51] The activation of this pathway could increase TGF-β expression by regulating the transglutaminase promoter, which is a potential inductor of TGF-β,[52] inducing ICAM-1 up-regulation,[53] and inducing feedback loops to further increase the activation of the NF-κB pathway, promote the accumulation of ECMs, including FN and collagens, and then promote the fibrosis process. Thus, to investigate the hypothesis that the TIF induced by MSNs is associated with inflammation, we measured the activation of the NF-κB inflammatory pathway. The results showed that MSNs activated the NF-κB pathway from the top down in NRK-52E cells within a short incubation time (Figure 7A), induced the nuclear translocation of NF-κB p65 (Figure 7B), and increased the expression of NF-κB target genes, including TNF-α and IL-1β in both a dose- and time-dependent manner; however, the activation of IL-6 was not significant, which may suggest the increase of NF-κB target genes was an alternative (Figure 7E and F). It has been reported that vitreous Si and pure quartz exhibit marked cytotoxicity resulting in the release of nitrite and TNF-α, suggesting a common behavior in the induction of oxidative stress.[54] Because activation of the NF-κB pathway and the transcription of early target genes downstream of this pathway is important in the inflammatory process,[55] the release of TNF-α could reactivate the NF-κB pathway by acting on the TNF-α receptor in the membrane. Thus, the feedback induced by the release of inflammatory cytokines positively affected the activation of the NF-κB pathway (Figure 7C and D). In fact, the persistent activation of the NF-κB pathway is simply a necessary condition of fibrosis development.[56] Moreover, the nuclear translocation of NF-κB p65 was also induced in the kidney homogenate after exposure (Figure 4B). These results raise the possibility that MSNs can activate the NF-κB pathway, and we presumed that this activation may mediate the development of TIF.

To investigate the role of the NF-κB pathway in the TIF caused by MSNs, we used BAY 11-7082, an inhibitor of the NF-κB pathway. This inhibitor can effectively prevent the phosphorylation of IκBα by cytokines and thereby decrease the nuclear translocation of NF-κB p65. In the process of TIF in other kidney diseases, activation of the NF-κB pathway may increase the expression of fibrosis markers, such as FN, TGF-β, and ICAM-1.[57–59] Herein, BAY 11-7082 decreased the degradation of IκBα and the nuclear translocation of p65 (Figure 8A and B), as well as the expression of NF-κB target genes (Figure 8D), and reversed the upregulation of FN, TGF-β, and ICAM-1 induced by MSNs (Figure 8C). These results indicate that inhibition of the NF-κB pathway could alleviate the fibrosis caused by MSNs and imply that the NF-κB pathway is involved in the development of TIF.

In summary, we revealed that a high dose of MSNs induces selective and acute nephrotoxicity and TIF in mice and RTECs and that the observed fibrosis is closely related to the NF-κB inflammatory signaling pathway. Due to their potential applications in various areas of biology and in disease diagnosis and treatment, the biocompatibility of MSNs has attracted increased attention.[60–63] In this work, a high dose was chosen to reflect the accumulation and the toxicity of MSNs in the kidney. Due to the diversity of the systemic phenotypic response and the translation of the physiologic/anatomic influence from animal models to human, an in vivo experimental evaluation of the nanotoxicology using appropriate dosing amounts may carry greater significance. This work provides additional experimental data to assess the biocompatibility of MSNs in vivo and in vitro and provides useful information to address the deficiency in the rapidly evolving area of human exposure to MSNs. We expect that further studies of the nanotoxicology mechanisms will promote the development of low-toxic and effective MSNs.

Conclusion

In conclusion, we have shown that MSNs intraperitoneally administered to mice have the potential to cause selective AKI at the early stage and result in the development of TIF. The obtained in vitro results suggest that the persistent activation of the NF-κB inflammatory pathway induced by MSNs could result in TIF progression in mice. We expect that this work will contribute to the development of drug delivery systems using MSNs.

Acknowledgment

This work was supported by the Key Projects in the National Science and Technology Pillar Program of China (Grant No 2008BAI55B03).

Disclosure

The authors report no conflicts of interest in this work.

References

1. Vallhov H, Gabrielsson S, Strømme M, Scheynius A, Garcia-Bennett AE. Mesoporous silica particles induce size dependent effects on human dendritic cells. *Nano Lett*. 2007;7(12):3576–3582.
2. Chung TH, Wu SH, Yao M, et al. The effect of surface charge on the uptake and biological function of mesoporous silica nanoparticles in 3T3-L1 cells and human mesenchymal stem cells. *Biomaterials*. 2007; 28(19):2959–2966.
3. Carino IS, Pasqua L, Testa F, et al. Silica-based mesoporous materials as drug delivery system for methotrexate release. *Drug Deliv*. 2007;14(8):491–495.
4. Gu J, Fan W, Shimojima A, Okubo T. Organic-inorganic mesoporous nanocarriers integrated with biogenic ligands. *Small*. 2007;3(10): 1740–1744.
5. Yun HS, Park JW, Kim SH, Kim YJ, Jang JH. Effect of the pore structure of bioactive glass balls on biocompatibility in vitro and in vivo. *Acta Biomater*. 2011;7(6):2651–2660.
6. Cainelli F, Tanko MN, Vento S. Vento, Silica exposure and silicosis: action is needed now. *South Med J*. 2010;103(11):1078.
7. DeMuth P, Hurley M, Wu C, et al. Mesoscale porous silica as drug delivery vehicles: Synthesis, characterization, and pH-sensitive release profiles. *Microporous and Mesoporous Materials*. 2011;141(1): 128–134.
8. Yuan L, Tang Q, Yang D, Zhang JZ, Zhang F, Hu J. Preparation of pH-responsive mesoporous silica nanoparticles and their application in controlled drug delivery. *The Journal of Physical Chemistry C*. 2011; 115(20):7.
9. Wang T, Chai F, Fu Q, et al. Uniform hollow mesoporous silica nanocages for drug delivery in vitroand in vivo for liver cancer therapy. *Journal of Materials Chemistry*. 2011;21(14):5299–5306.
10. He Q, Shi J. Mesoporous silica nanoparticle based nano drug delivery systems: synthesis, controlled drug release and delivery, pharmacokinetics and biocompatibility. *Journal of Materials Chemistry*. 2011;21(16):5845–5855.
11. Lee S, Yun HS, Kim SH. The comparative effects of mesoporous silica nanoparticles and colloidal silica on inflammation and apoptosis. *Biomaterials*. 2011;32(35):9434–9443.
12. Lu J, Liong M, Li Z, Zink JI, Tamanoi F. Biocompatibility, Biodistribution, and Drug-Delivery Efficiency of Mesoporous Silica Nanoparticles for Cancer Therapy in Animals. *Small*. 2010;6(16): 1794–1805.
13. Yu T, Greish K, McGill LD, Ray A, Ghandehari H. Influence of geometry, porosity, and surface characteristics of silica nanoparticles on acute toxicity: their vasculature effect and tolerance threshold. *ACS Nano*. 2012;6(3):2289–2301.
14. Wang F, Gao F, Lan M, Yuan H, Huang Y, Liu J. Oxidative stress contributes to silica nanoparticle-induced cytotoxicity in human embryonic kidney cells. *Toxicol In Vitro*. 2009;23(5):808–815.
15. Passagne I, Morille M, Rousset M, Pujalté I, L'azou B. Implication of oxidative stress in size-dependent toxicity of silica nanoparticles in kidney cells. *Toxicology*. 2012;299(2–3):112–124.
16. Karin M, Ben-Neriah Y. Phosphorylation meets ubiquitination: the control of NF-[kappa]B activity. *Annu Rev Immunol*. 2000;18:621–663.
17. Bierhaus A, Schiekofer S, Schwaninger M, et al. Diabetes-associated sustained activation of the transcription factor nuclear factor-kappaB. *Diabetes*. 2001;50(12):2792–2808.
18. Rial NS, Choi K, Nguyen T, Snyder B, Slepian MJ. Nuclear factor kappaB (NF-κB): a novel cause for diabetes, coronary artery disease and cancer initiation and promotion? *Med Hypotheses*. 2012;78(1):29–32.
19. Schmid H, Boucherot A, Yasuda Y, et al. Modular activation of nuclear factor-kappaB transcriptional programs in human diabetic nephropathy. *Diabetes*. 2006;55(11):2993–3003.
20. Li L, Tang F, Liu H, et al. In vivo delivery of silica nanorattle encapsulated docetaxel for liver cancer therapy with low toxicity and high efficacy. *ACS Nano*. 2010;4(11):6874–6882.
21. Lu J, Liong M, Zink JI, Tamanoi F. Mesoporous silica nanoparticles as a delivery system for hydrophobic anticancer drugs. *Small*. 2007; 3(8):1341–1346.
22. Wang QX, Xiang Y, Cui YL, Lin KM, Zhang XF. Dietary blue pigments derived from genipin, attenuate inflammation by inhibiting LPS-induced iNOS and COX-2expression via the NF-κB inactivation. *PLoS One*. 2012;7(3):e34112.
23. Zhang JY, Jin H, Wang GF, et al. Methyl-1-hydroxy-2-naphthoate, a novel naphthol derivative, inhibits lipopolysaccharide-induced inflammatory response in macrophages via suppression of NF-κB, JNK and p38 MAPK pathways. *Inflamm Res*. 2011;60(9):851–859.
24. Wang LY, Wang HY, Ouyang J, et al. Low concentration of lipopolysaccharide acts on MC3T3-E1 osteoblasts and induces proliferation via the COX-2-independent NFkappaB pathway. *Cell Biochem Funct*. 2009;27(4):238–242.
25. Liu H, Chen D, Li L, et al. Multifunctional gold nanoshells on silica nanorattles: a platform for the combination of photothermal therapy and chemotherapy with low systemic toxicity. *Angew Chem Int Ed Engl*. 2011;50(4):891–895.
26. Hamilton RF Jr, Thakur SA, Mayfair JK, Holian A. MARCO mediates silica uptake and toxicity in alveolar macrophages from C57BL/6 mice. *J Biol Chem*. 2006;281(45):34218–3426.
27. Slowing II, Vivero-Escoto JL, Wu CW, Lin VS. Mesoporous silica nanoparticles as controlled release drug delivery and gene transfection carriers. *Adv Drug Deliv Rev*. 2008;60(11):1278–1288.
28. Slowing II, Wu CW, Vivero-Escoto JL, Lin VS. Mesoporous silica nanoparticles for reducing hemolytic activity towards mammalian red blood cells. *Small*. 2009;5(1):57–62.
29. Tao Z, Morrow MP, Asefa T, et al. Mesoporous silica nanoparticles inhibit cellular respiration. *Nano Lett*. 2008;8(5):1517–1526.
30. Bellusci M, La Barbera A, Padella F, et al. Biodistribution and acute toxicity of a nanofluid containing manganese iron oxide nanoparticles produced by a mechanochemical process. *Int J Nanomedicine*. 2014;9:1919–1929.
31. Mancuso L, Cao G. Acute toxicity test of CuO nanoparticles using human mesenchymal stem cells. *Toxicol Mech Methods*. 2014;24(7): 449–554.
32. Lorke D. A new approach to practical acute toxicity testing. *Arch Toxicol*. 1983;54(4):275–287.
33. International conference on harmonisation. *ICH guidance on toxicokinetics: the assessment of systemic exposure in toxicity studies s3a*; 1994. Available from: http://www.ich.org/fileadmin/Public_Web_Site/ICH_Products/Guidelines/Safety/S3A/Step4/S3A_Guideline.pdf. Accessed November 15, 2014.

34. The Organisation for Economic Co-operation and Development. *OECD guidelines for the testing of the chemicals-draft proposal for a revised TG 417: Toxicokinetics*; 2008. Available from: http://www.oecd.org/chemicalsafety/testing/41690691.pdf. Accessed November 15, 2014.
35. United States Food and Drug Administration. *M3(R2) nonclinical safety studies for the conduct of human clinical trials and marketing authorization for pharmaceuticals*; 2010. Available from: http://www.fda.gov/downloads/drugs/guidancecomplianceregulatoryinformation/guidances/ucm073246.pdf. Accessed November 15, 2014.
36. United States Food and Drug Administration. *Guidance for industry, developing medical imaging drug and biological products, part 1: conducting safety assessments*; 2004. Available from: http://www.fda.gov/downloads/Drugs/.../Guidances/ucm071600.pdf. Accessed November 15, 2014.
37. Kanakia S, Toussaint JD, Mullick Chowdhury S, et al. Dose ranging, expanded acute toxicity and safety pharmacology studies for intravenously administered functionalized graphene nanoparticle formulations. *Biomaterials*. 2014;35(25):7022–7031.
38. Eddy AA. Molecular basis of renal fibrosis. *Pediatr Nephrol*. 2000; 15(3–4):290–301.
39. Leung KC, Tonelli M, James MT. Chronic kidney disease following acute kidney injury-risk and outcomes. *Nat Rev Nephrol*. 2013;9(2): 77–85.
40. Souris JS, Lee CH, Cheng SH, et al. Surface charge-mediated rapid hepatobiliary excretion of mesoporous silica nanoparticles. *Biomaterials*. 2010;31(21):5564–5574.
41. Nabeshi H, Yoshikawa T, Matsuyama K, et al. Systemic distribution, nuclear entry and cytotoxicity of amorphous nanosilica following topical application. *Biomaterials.* 2011;32(11):2713–2724.
42. Nabeshi H, Yoshikawa T, Matsuyama K, et al. Amorphous nanosilicas induce consumptive coagulopathy after systemic exposure. *Nanotechnology.* 2012;23(4):045101.
43. Yoshida T, Yoshioka Y, Tochigi S, et al. Intranasal exposure to amorphous nanosilica particles could activate intrinsic coagulation cascade and platelets in mice. *Part Fibre Toxicol*. 2013;10:41.
44. Liu T, Li L, Fu C, Liu H, Chen D, Tang F. Pathological mechanisms of liver injury caused by continuous intraperitoneal injection of silica nanoparticles. *Biomaterials*. 2012;33(7):2399–2407.
45. Tao Z, Toms BB, Goodisman J, Asefa T. Mesoporosity and functional group dependent endocytosis and cytotoxicity of silica nanomaterials. *Chem Res Toxicol*. 2009;22(11):1869–1880.
46. Sun W, Fang N, Trewyn BG, et al. Endocytosis of a single mesoporous silica nanoparticle into a human lung cancer cell observed by differential interference contrast microscopy. *Anal Bioanal Chem*. 2008; 391(6):2119–2125.
47. Harrison J, Chen JQ, Miller W, et al. Risk of silicosis in cohorts of Chinese tin and tungsten miners and pottery workers (II): Workplace-specific silica particle surface composition. *Am J Ind Med*. 2005; 48(1):10–15.
48. Mundt KA, Birk T, Parsons W, et al. Respirable crystalline silica exposure-response evaluation of silicosis morbidity and lung cancer mortality in the German porcelain industry cohort. *J Occup Environ Med*. 2011;53(3):282–289.
49. Mühlfeld C, Gehr P, Rothen-Rutishauser B. Translocation and cellular entering mechanisms of nanoparticles in the respiratory tract. *Swiss Med Wkly*. 2008;138(27–28):387–391.
50. Oberdörster G, Oberdörster E, Oberdörster J. Nanotoxicology: an emerging discipline evolving from studies of ultrafine particles. *Environ Health Perspect*. 2005;113(7):823–839.
51. Guijarro C, Egido J. Transcription factor-kappaB (NF-kappaB) and renal disease. *Kidney Int*. 2001;59(2):415–424.
52. Bitzer M, von Gersdorff G, Liang D, et al. A mechanism of suppression of TGF-beta/SMAD signaling by NF-kappaB/RelA. *Genes Dev*. 2000;14(2):187–197.
53. Chen L, Zhang J, Zhang Y, Wang Y, Wang B. Improvement of inflammatory responses associated with NF-kappaB pathway in kidneys from diabetic rats. *Inflamm Res*. 2008;57(5):199–204.
54. Ghiazza M, Polimeni M, Fenoglio I, Gazzano E, Ghigo D, Fubini B. Does vitreous silica contradict the toxicity of the crystalline silica paradigm? *Chem Res Toxicol*. 2010;23(3):620–629.
55. Kang JL, Jung HJ, Lee K, Kim HR. Src tyrosine kinases mediate crystalline silica-induced NF-kappaB activation through tyrosine phosphorylation of IkappaB-alpha and p65 NF-kappaB in RAW 264.7 macrophages. *Toxicol Sci*. 2006;90(2):470–477.
56. Mirza A, Liu SL, Frizell E, et al. A role for tissue transglutaminase in hepatic injury and fibrogenesis, and its regulation by NF-kappaB. *Am J Physiol*. 1997;272(2 Pt 1):G281–G288.
57. Bondar' IA, Klimontov VV, Nadeev AP. [Urinary excretion of proinflammatory cytokines and transforming growth factor beta at early stages of diabetic nephropathy]. *Ter Arkh*. 2008;80(1):52–56. Russian.
58. Iwamoto M, Mizuiri S, Arita M, Hemmi H. Nuclear factor-kappaB activation in diabetic rat kidney: evidence for involvement of P-selectin in diabetic nephropathy. *Tohoku J Exp Med*. 2005;206(2):163–171.
59. Mezzano S, Aros C, Droguett A, et al. NF-kappaB activation and overexpression of regulated genes in human diabetic nephropathy. *Nephrol Dial Transplant*. 2004;19(10):2505–2512.
60. Huang X, Zhuang J, Teng X, et al. The promotion of human malignant melanoma growth by mesoporous silica nanoparticles through decreased reactive oxygen species. *Biomaterials*. 2010;31(24):6142–2153.
61. Huang X, Teng X, Chen D, Tang F, He J. The effect of the shape of mesoporous silica nanoparticles on cellular uptake and cell function. *Biomaterials*. 2010;31(3):438–448.
62. Angelos SL, Liong M, Choi E, Zink JI. Mesoporous silicate materials as substrates for molecular machines and drug delivery. *Chemical Engineering Journal*. 2008;137:4–13.
63. Huang X, Zhuang J, Chen D, et al. General strategy for designing functionalized magnetic microspheres for different bioapplications. *Langmuir*. 2009;25(19):11657–11663.

Supplementary materials

Table S1 LD_{50} of MSNs in mice

Dose (mg/kg)	Animals	Life(O)/Death(X)	LD_{50} (mg/kg)	95% CI (mg/kg)
1,000	3	XXX		
800	4	OOOX	800	609.1–1,130
640	1	O		

Abbreviations: MSNs, mesoporous silica nanoparticles; CI, confidence interval; LD_{50}, lethal dosage.

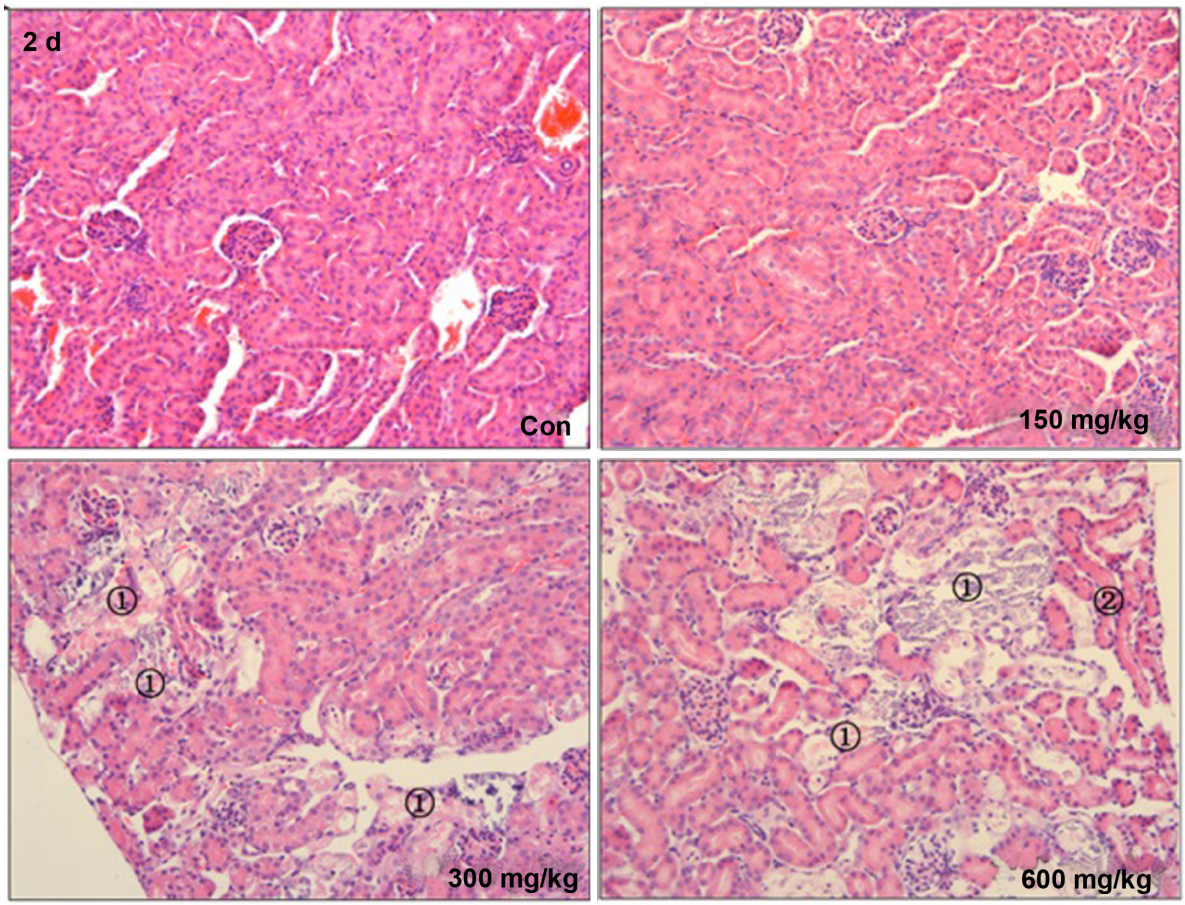

Figure S1 Original images of Figure 3A.
Abbreviations: d, day(s); con, control.

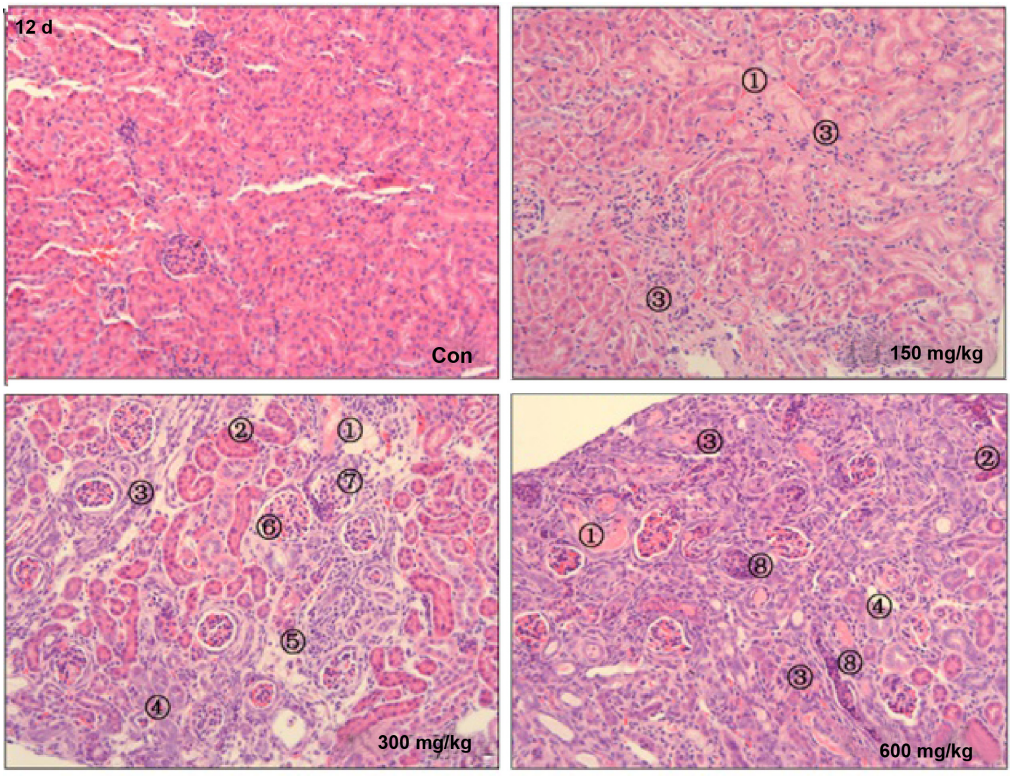

Figure S2 Original images of Figure 3B.
Abbreviations: d, day(s); con, control.

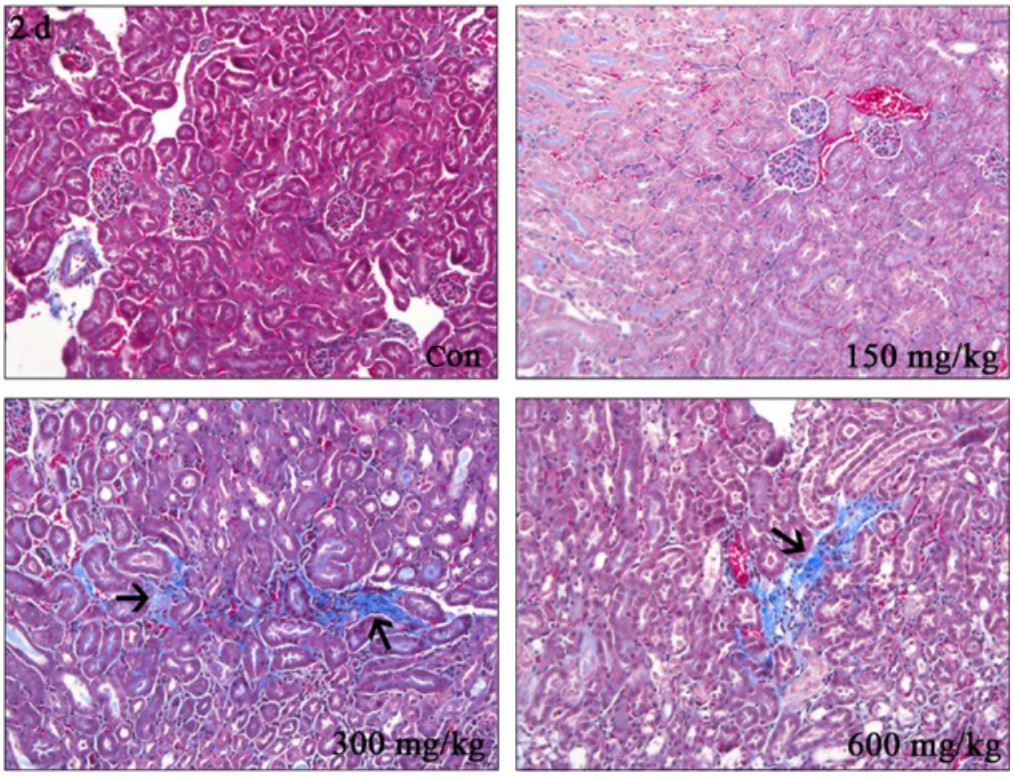

Figure S3 Original images of Figure 3C.
Abbreviations: d, day(s); con, control.

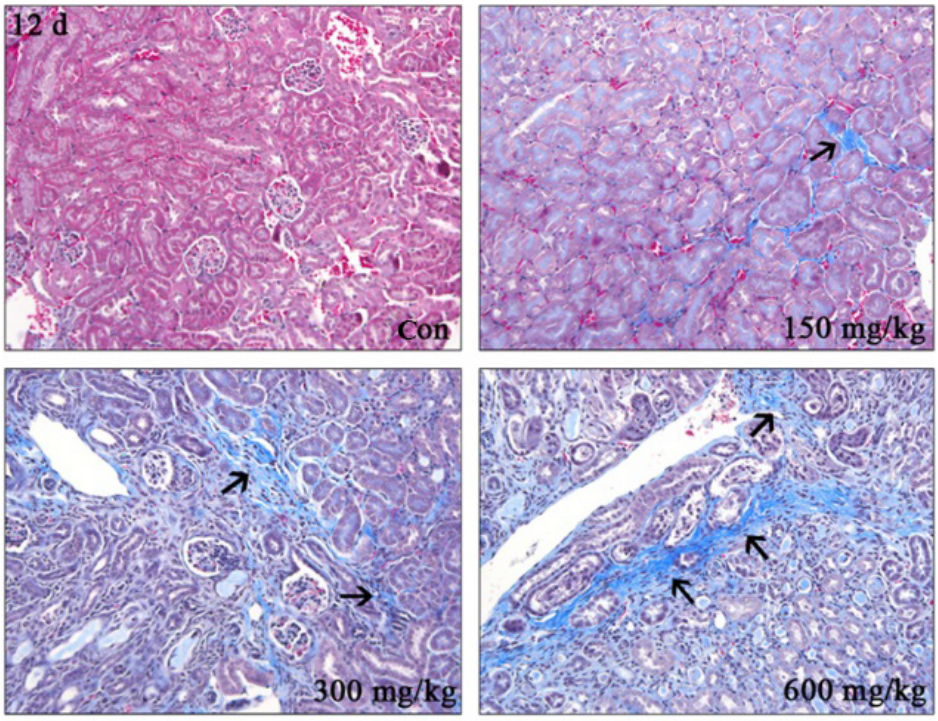

Figure S4 Original images of Figure 3D.
Abbreviations: d, day(s); con, control.

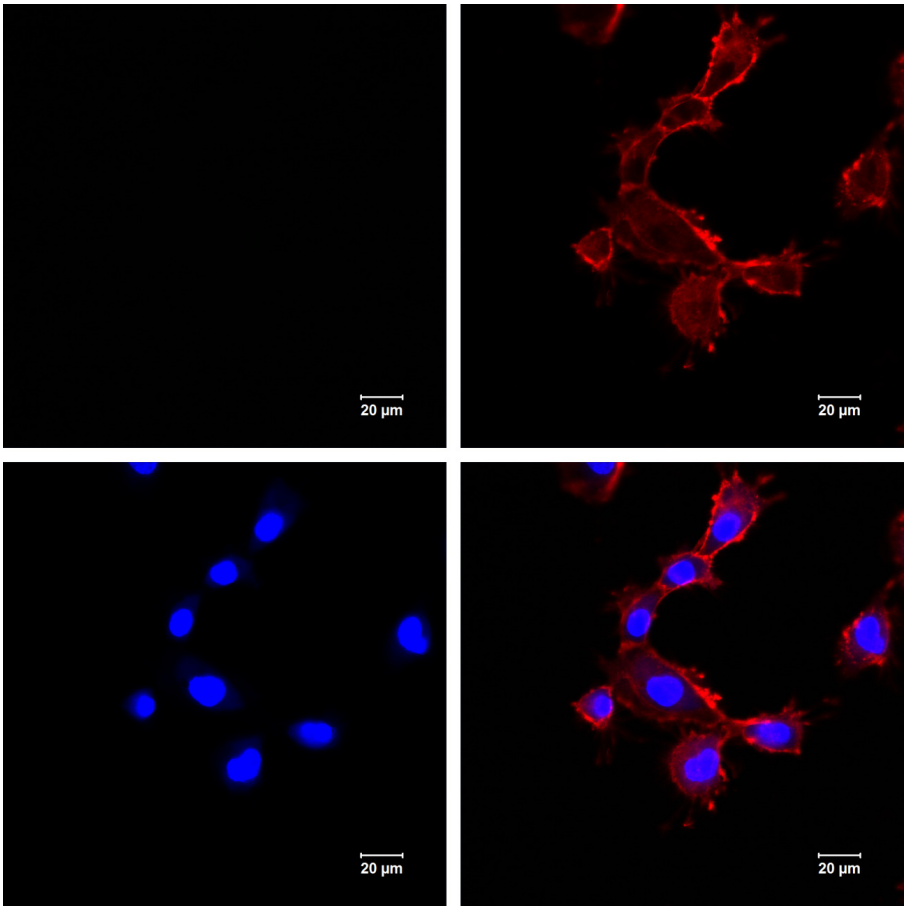

Figure S5 Original images of Figure 5C – con.
Abbreviation: con, control.

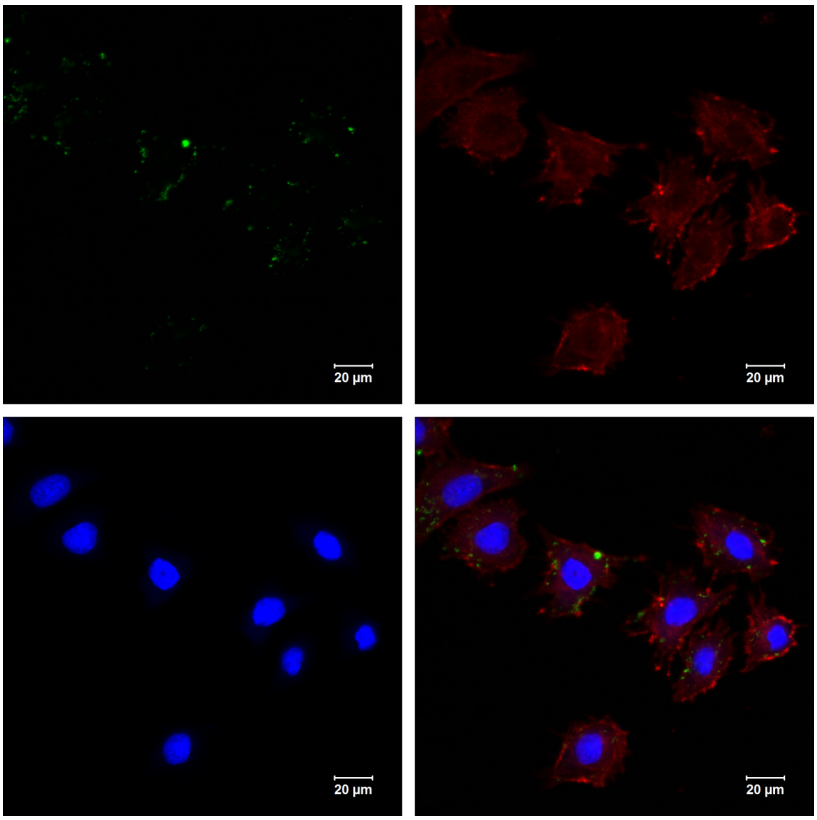

Figure S6 Original images of Figure 5C – 15 minutes.

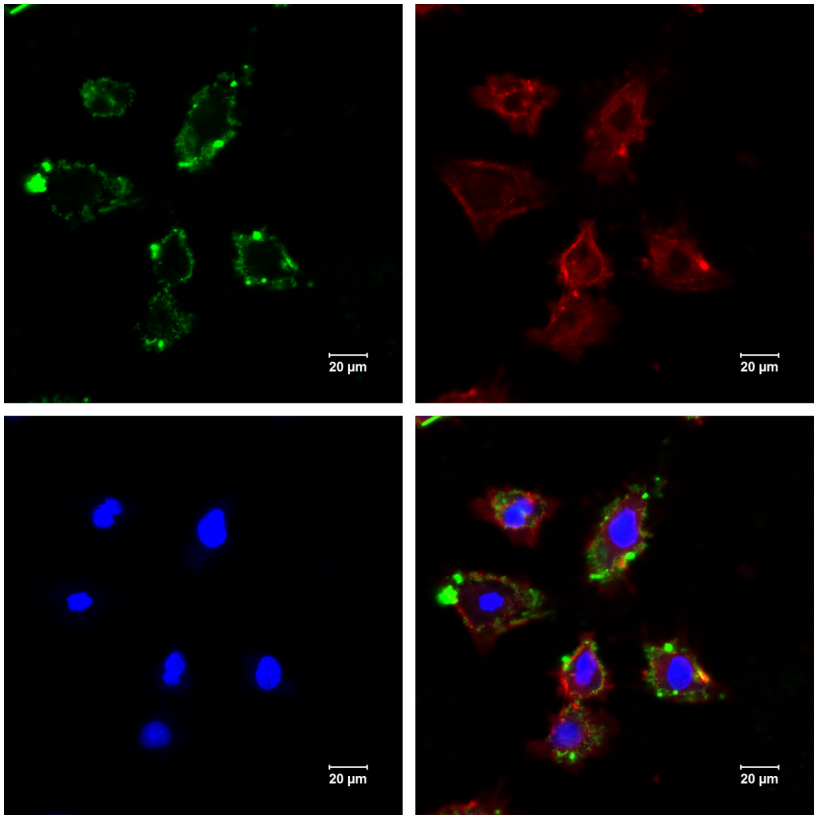

Figure S7 Original images of Figure 5C – 30 minutes.

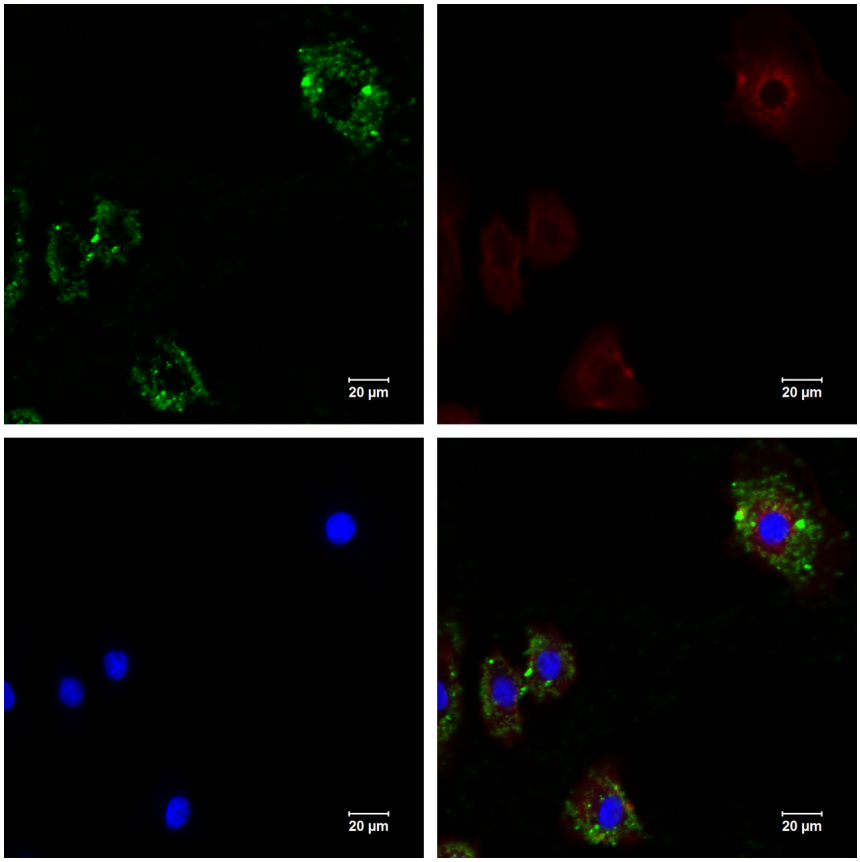

Figure S8 Original images of Figure 5C – 180 minutes.